

Redox Shuttle-Based Electrolytes for Dye-Sensitized Solar Cells: Comprehensive Guidance, Recent Progress, and Future Perspective

Masud and Hwan Kyu Kim*

Cite This: *ACS Omega* 2023, 8, 6139–6163

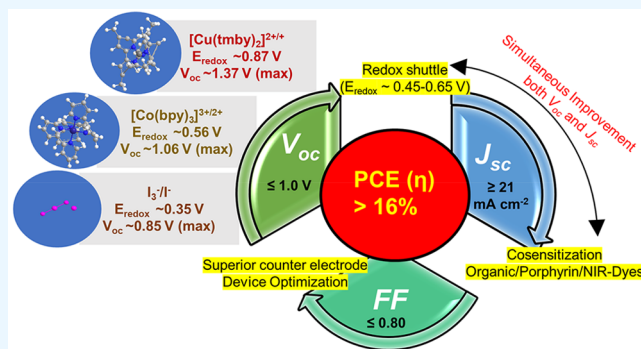
Read Online

ACCESS |

Metrics & More

Article Recommendations

ABSTRACT: A redox electrolyte is a crucial part of dye-sensitized solar cells (DSSCs), which plays a significant role in the photovoltage and photocurrent of the DSSCs through efficient dye regeneration and minimization of charge recombination. An I^-/I_3^- redox shuttle has been mostly utilized, but it limits the open-circuit voltage (V_{oc}) to 0.7–0.8 V. To improve the V_{oc} value, an alternative redox shuttle with more positive redox potential is required. Thus, by utilizing cobalt complexes with polypyridyl ligands, a significant power conversion efficiency (PCE) of above 14% with a high V_{oc} of up to 1 V under 1-sun illumination was achieved. Recently, the V_{oc} of a DSSC has exceeded 1 V with a PCE of around 15% by using Cu-complex-based redox shuttles. The PCE of over 34% in DSSCs under ambient light by using these Cu-complex-based redox shuttles also proves the potential for the commercialization of DSSCs in indoor applications. However, most of the developed highly efficient porphyrin and organic dyes cannot be used for the Cu-complex-based redox shuttles due to their higher positive redox potentials. Therefore, the replacement of suitable ligands in Cu complexes or an alternative redox shuttle with a redox potential of 0.45–0.65 V has been required to utilize the highly efficient porphyrin and organic dyes. As a consequence, for the first time, the proposed strategy for a PCE enhancement of over 16% in DSSCs with a suitable redox shuttle is made by finding a superior counter electrode to enhance the fill factor and a suitable near-infrared (NIR)-absorbing dye for cosensitization with the existing dyes to further broaden the light absorption and enhance the short-circuit current density (J_{sc}) value. This review comprehensively analyzes the redox shuttles and redox-shuttle-based liquid electrolytes for DSSCs and gives recent progress and perspectives.



1. INTRODUCTION

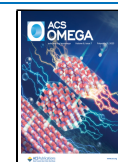
Solar energy, which comes from radiant light and heat from the sun, is the most powerful source of renewable energy. Solar energy is about 200 times greater than all renewable energy resources combined.¹ The most efficient way to harness solar energy is through photovoltaic technology that directly converts sunlight into electrical energy. Among various emerging photovoltaic technologies, dye-sensitized solar cells (DSSCs) have received great attention due to several advantages, such as facile cell fabrication, low cost, multicoloration appropriate for building and automobile integration, high power conversion efficiency (PCE) under outdoor and indoor light, and so on. Figure 1 shows the device structure of a DSSC and its working principle. The working electrode, also known as the photoanode, consists of a dye-sensitized thin film of a wide-band-gap semiconducting material (mostly n-type TiO_2) with a nanocrystalline morphology deposited on a transparent conducting oxide (TCO) coated glass substrate. The counter electrode consists of a TCO substrate coated with a suitable catalyst (usually Pt). Redox liquid electrolytes contain a redox couple as a redox shuttle in the most common

organic solvent medium. A DSSC works through several charge transfer processes: dye excitation, charge injection and transportation, dye regeneration, and electrolyte regeneration. In the first step, the dye absorbs photons, and electrons from the HOMO (highest occupied molecular orbital) level move to the LUMO (lowest unoccupied molecular orbital) level. Then the excited dye injects electrons in the LUMO level into the conduction band of the TiO_2 semiconductor. As a result, a charge separation occurs at the interface of the dye and the wide-band-gap nanostructured TiO_2 semiconductor. Then, the TiO_2 semiconductor transports electrons quickly to the FTO electrode through diffusion, and these electrons move to the counter electrode through an external circuit.

Received: October 24, 2022

Accepted: January 20, 2023

Published: February 6, 2023



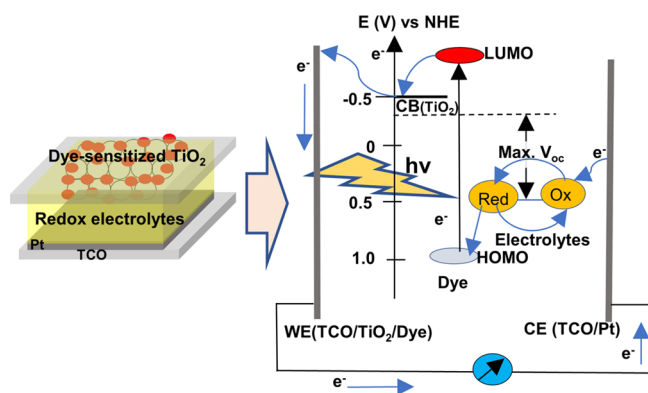


Figure 1. DSSC device structure with an n-type TiO_2 semiconductor and its working principle.

The oxidized dye regenerates by obtaining electrons from reduced species of electrolytes, which are oxidized. The oxidized species of electrolytes move toward the counter electrodes through diffusion, where these species receive electrons that come from the anode through an external circuit. This step is called electrolyte regeneration.

Besides the charge transfer processes required above, there is also the possibility of losing injected electrons by the oxidized dye and oxidized species of electrolytes. This undesirable back-charge-transfer process is called charge recombination. The dye regeneration should be fast to avoid injected electron recombination with the oxidized dye.

In indoor photovoltaics, DSSCs are promising candidates for commercialization due to the outstanding PCE (above 34%) and the great long-term device stability under ambient conditions. The Japanese electronics company Ricoh has already launched a 20% efficiency indoor photovoltaic solid-state dye-sensitized solar cell for integration with IoT sensors and autonomous electronic devices that require low electricity to power them.² The Swedish company Exeger has already started the commercialization and integration of the DSSC technology within electronic devices that can generate power from indoor and outdoor light. By utilizing DSSC materials, this company makes Powerfoyle, a unique environment-friendly material that converts light into electricity and is capable of charging electronic devices with daylight and indoor light.³

In the last three decades, significant progress has been achieved in the DSSC field using D- π -A-structured organic and porphyrin dyes,^{4–7} cosensitized dyes,^{8–12} replacing redox mediators,^{13–18} solidifying liquid electrolytes,^{19–21} and developing counter electrode catalysts.^{22–27} A redox electrolyte is the vital component of a DSSC which affects the cell performance and long-term stability of the device. An electrolyte is accountable for the regeneration of photo-oxidized dye to dye and the transportation of the inner charge carrier between electrodes. Three parameters, photocurrent density (J_{sc}), photovoltage (V_{oc}), and fill factor (FF), determine the PCE of the device. Electrolytes play a key role in contributing all three parameters (J_{sc} , V_{oc} , and FF) of the device. Iodine electrolyte has been employed as the most widely used redox shuttle in DSSCs, and a maximum PCE of 12.4% under 1-sun illumination was achieved with concerted companion dyes.^{10,28} The low positive redox potential of the I^-/I_3^- redox shuttle limits the open-circuit voltage (V_{oc}) to 0.7–0.8 V since the V_{oc} value is typically determined by the

potential difference between the quasi-Fermi energy level of TiO_2 and the redox potential of redox shuttles. Furthermore, competitive light absorption, the volatile nature of iodine, and corrosiveness toward metals, especially Ag, limit the iodine electrolytes for module development. Transition-metal complexes, especially Co complexes, have received great attention as redox shuttles due to the enhancement of the open-circuit voltage (V_{oc}) of the device. Although the PCE of DSSCs under simulated 1-sun illumination has reached over 14% using cobalt electrolytes,^{9,11} sluggish mass transport and large reorganization between d^7 (high-spin) and d^6 (low-spin) in Co complexes limit a high V_{oc} to 1 V. Recently, Cu complexes have been received great attention and recorded a PCE of 15.2% with a higher V_{oc} of over 1 V obtained under simulated 1-sun irradiation by using a $[\text{Cu}(\text{tmby})_2]^+ / [\text{Cu}(\text{tmby})_2]^{2+}$ redox shuttle with cosensitized organic dyes.²⁹ Further improvement of PCE under 1-sun illumination is challenging by this $[\text{Cu}(\text{tmby})_2]^+ / [\text{Cu}(\text{tmby})_2]^{2+}$ redox shuttle, because an improvement in J_{sc} value by using this redox shuttle is difficult.³⁰ The competitive light absorption of Cu complexes with the dye in the blue region of the visible light spectrum and the use of a dye with a higher positive HOMO level reduce the entire visible light absorption range, which limits the J_{sc} value. Therefore, tuning the redox potential ($E_{\text{redox}} \approx 0.45\text{--}0.65$ V vs NHE) of the Cu complexes by varying ligands, such as pentadentate ligands,³⁰ can be a better solution so that currently developed porphyrin, organic, and NIR-absorbing dyes can be utilized for cosensitization with a Cu complex redox shuttle. Additionally, to enhance the long-term stability of the device, sealing with advanced techniques, such as glass frit encapsulation,^{31,32} and development of solidifying agents, such as polymeric gelating materials,^{19,33} to reduce the volatile organic solvent are also essential. This review comprehensively analyzes the DSSC redox liquid electrolytes (LEs) with advances and perspectives. According to our perspective, above 16% PCE under 1-sun is feasible to achieve for DSSCs, which is depicted and discussed in **Summary and Outlook**.

2. SOLAR CELL EVALUATION

The dye-sensitized solar cell can be electrically modeled with the equivalent circuit shown in **Figure 2**, by including series resistance (R_s) and shunt resistance (R_{sh}).

The derived characteristic current density (J)–voltage (V) equation from the modified Shockley diode equation for the solar cell based on the equivalent circuit (see **Figure 2**) is expressed as

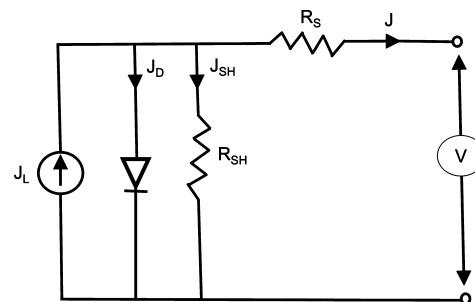


Figure 2. Modified diode equivalent circuit for the dye-sensitized solar cell.

$$J = J_L - J_0 \left\{ \exp \left(\frac{q(V + JR_S)}{nkT} \right) - 1 \right\} - \frac{V + JR_S}{R_{SH}} \quad (1)$$

where J_L is the photogenerated current density, J_0 is the dark saturation current density, n is the diode ideality factor, R_S and R_{SH} are the series resistance and shunt resistance, respectively, q is the elementary charge (1.6×10^{-19} C), k is the Boltzmann constant (1.38×10^{-23} m² kg s⁻² K⁻¹), and T is the absolute temperature.

The photovoltaic performance of DSSCs is estimated from J - V characteristics measurement under light illumination. The power conversion efficiency (PCE, denoted by η) of DSSC is evaluated from the J - V curve (Figure 3) by the eq 2

$$\eta = \frac{J_{sc} V_{oc} FF}{P_{in}} \quad (2)$$

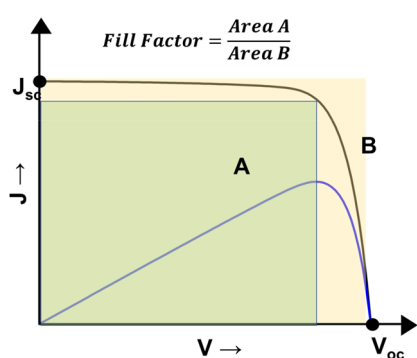


Figure 3. J - V curve of the DSSC.

where J_{sc} is the short-circuit current density, V_{oc} is the open-circuit voltage, FF is the fill factor, and P_{in} is the incident light power density for the J - V curve measurement.

2.1. Short-Circuit Current Density (J_{sc}). Under short-circuit conditions, charges generated by photon absorption should flow into the external circuit with unit efficiency. The current density in the DSSC with incident light illumination of photon flux $\phi(\lambda)$ under a short-circuit condition is given by eq 3:^{34,35}

$$\begin{aligned} J_{sc} &= q_e \int_{\lambda_{min}}^{\lambda_{max}} \text{IPCE}(\lambda) \phi(\lambda) d\lambda \\ &= q_e \int_{\lambda_{min}}^{\lambda_{max}} \text{LHE}(\lambda) \Phi_{inj} \eta_{reg} \eta_{cc} \phi(\lambda) d\lambda \end{aligned} \quad (3)$$

Here, the monochromatic incident-photon-to-current conversion efficiency (IPCE(λ)) is related to the light-harvesting efficiency (LHE) of the dye, the electron injection efficiency (Φ_{inj}) in the excited state, the dye regeneration efficiency (η_{reg}) by electrolytes, and the charge collection efficiency (η_{cc}) of the TiO_2 electrode.

The LHE or absorbance ($\alpha(\lambda)$) can be expressed by eq 4:³⁶

$$\text{LHE} = 1 - 10^{-A(\lambda)} \quad (4)$$

where $A(\lambda)$ is the absorbance of the dye related to the molar extinction coefficient and the surface area of the loaded dye, as expressed in eq 5

$$A(\lambda) = \log \left(\frac{I_0(\lambda)}{I(\lambda)} \right) = -1000 \epsilon(\lambda) \frac{1}{A_{dye}} \quad (5)$$

where $I_0(\lambda)$ and $I(\lambda)$ are the incident and transmitted light through the sample, respectively.

Thus, the LHE is influenced by the light absorption range of the dye, the amount of dye loaded in the mesoporous TiO_2 surface, and the intensity of the incident light (see eqs 4 and 5). Usually, the surface area of the mesoporous TiO_2 film is high; therefore, a large amount of dye can be loaded or adsorbed on the TiO_2 film. Typically, the mesoporous TiO_2 film has 18–20 nm diameter TiO_2 nanoparticles that are much smaller than the wavelength of visible light. The scattering of light by the mesoporous TiO_2 film can reduce the LHE by about 5%.³⁷ Therefore, the optimization and improvement of the TiO_2 film by having a scattering layer with larger TiO_2 nanoparticles (typically ~ 400 nm) can reduce light scattering and improve the LHE. Dye aggregation and charge recombination are two negative factors that can significantly reduce the LHE.

The electron injection efficiency (Φ_{inj}) depends on the free energy change (ΔG_{inj}) for the electron transfer from the excited dye to the TiO_2 semiconductor conduction band. ΔG_{inj} is expressed by eq 6

$$\Delta G_{inj} = E_{dye^*(\text{LUMO})} - E_{CB} \quad (6)$$

where $E_{dye^*(\text{LUMO})}$ is the oxidation potential of the excited dye, i.e., the energy of the lowest unoccupied molecular orbital of the dye, and E_{CB} is the energy of the conduction band edge of the semiconductor (typically 4.0 eV for anatase TiO_2). For an efficient Φ_{inj} , ΔG_{inj} should be > -0.2 eV.³⁷

Dye aggregation reduces the electron injection efficiency. The recombination of the injected electrons with the oxidized dye can reduce Φ_{inj} . The dye regeneration efficiency (η_{reg}) depends on the free energy change (ΔG_{reg}) in the reduction of the oxidized dye by the reduced species of electrolytes. ΔG_{reg} is expressed by eq 7

$$\Delta G_{reg} = E_{dye(\text{HOMO})} - E_{redox} \quad (7)$$

where $E_{dye(\text{HOMO})}$ is the ground-state oxidation potential, i.e., the energy of the highest occupied molecular orbital (HOMO) of the dye, and E_{redox} is the redox potential of the electrolytes. The dye regeneration by the reduced species of electrolytes should be fast for high-performance DSSCs. The redox potential of the redox shuttle should be higher (more negative) than the energy of the HOMO level of the dye to maintain the optimum driving force for efficient dye regeneration.

2.2. Open-Circuit Voltage (V_{oc}). Under an open-circuit condition, $I = 0$, the shunt resistance is assumed to be infinite. Thus, neglecting the final term of the J - V characteristics (eq 1), the open-circuit voltage (V_{oc}), which is the maximum voltage obtained from the solar cell, is given by eq 8

$$V_{oc} = \frac{nkT}{q} \ln \left(\frac{J_L}{J_0} + 1 \right) \approx \frac{kT}{q\beta} \ln \left(\frac{J_L}{J_0} \right) \quad (8)$$

Because $J_L \gg J_0$, therefore, $J_L + J_0 \approx J_L$.

The above equation for V_{oc} derived from the modified Shockley diode equation for the solar cell is also relevant for the V_{oc} value of the DSSC.

Under the open-circuit condition, the charges generated by the absorption of the photons recombine inside the cell. The photogenerated current density, J_L , depends on the IPCE spectrum. The ideality factor, n , depends on the nonlinear recombination in the cell, and the inverse of the ideality factor is called the back-reaction order, β . The dark saturation current

density, J_o , depends on the interfacial charge recombination of the cell and can be expressed by eq 9³⁸

$$J_o = n_o k_{\text{rec}} n_a \quad (9)$$

where n_o is the density of electrons in the conduction band state at thermal equilibrium accessible for the recombination under dark conditions, k_{rec} is the recombination rate, and n_a is the density of electron acceptors from the redox species of the electrolytes accessible for the recombination. Thus, by controlling or lowering the back-recombination (dark) reaction, it is possible to improve the V_{oc} of the device.

The electron concentration in thermal equilibrium, n_o , can be expressed by eq 10³⁸

$$n_o = N_c \exp\left(\frac{E_a - E_c}{\alpha kT}\right) \quad (10)$$

where N_c is the concentration of electrons in the conduction band/trap state, E_a and E_c are the energy levels of the semiconductor conduction band and redox species, respectively, and α is the tailing parameter related to the trap states.

Under light illumination, the concentration of free electrons (n) increases around to its equilibrium value, n_o . The V_{oc} value for the DSSC under constant light illumination can be obtained from the difference of the quasi-Fermi level (E_{Fn}) of the TiO₂ semiconductor and redox potential (E_{redox}) of the electrolytes.^{39,40}

$$V_{\text{oc}} = \frac{E_{\text{Fn}} - E_{\text{redox}}}{q} = \frac{kT}{q} \ln\left(\frac{n}{n_o}\right) \quad (11)$$

According to eqs 8–11, charge recombination, electron density in the trap, state semiconductor Fermi level, and the redox potential of the electrolytes can affect the V_{oc} value of the cell.

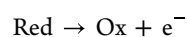
2.3. Fill Factor (FF). The fill factor (FF) is defined as the ratio of the maximum power obtained from the solar cell to the product of the J_{sc} and V_{oc} (see Figure 3). FF is regarded as the power efficiency of the solar cell. Electrical and electrochemical losses during in the solar cell operation influence FF.⁴¹ The shunt resistance (R_{SH}) in the DSSC originates from the resistance for electron recombination (back electron transfer) across TiO₂/electrolyte interfaces. The series resistance (R_{S}) comes from the contribution of the sheet resistance of FTO, the electron transport resistance in TiO₂, the mass transport of the electrolytes, and the charge transfer resistance at the counter electrode/electrolyte interfaces. The main contribution to the series resistance is the sheet resistance of the FTO substrate.^{42,43} A lower R_{S} and higher R_{SH} can give a higher fill factor. Generally, the fill factor of DSSCs varies from 0.6 to 0.8 because of the charge recombination and transport resistances.

3. REDOX ELECTROLYTES

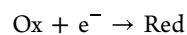
The redox electrolytes are the key components of the DSSC and have a substantial impact on both the performance and long-term stability of the device.⁴⁴ The liquid electrolytes (LEs) of DSSCs are liquid redox systems where the redox couple or shuttles are solvated in an aqueous or more common organic solvent medium.

3.1. Function of Redox Electrolytes in DSSCs. After photon absorption, the dye rapidly injects electrons from its excited state to the conduction band of the TiO₂ and oxidizes (see Figure 1). The oxidized dye receives electrons from the

reduced species in the electrolytes, which are oxidized by the following reaction:



In the counter electrode, a reverse reaction occurs:



The oxidized (Ox) species of the redox mediator migrate to the counter electrode and the reduced (Red) species of the redox mediator migrate from the counter electrode to the oxidized dye mainly through diffusion. The function of electrolytes in DSSCs is the dye regeneration and regeneration of reduced species of the redox couple in the counter electrode. The counter electrode requires the catalytic system to capture the electrons that come from the photoanode via the external circuit.

The photovoltaic performance of DSSCs strongly influences the kinetic competition of the dye regeneration reaction by the redox mediator and the injected electron recombination (dark reaction) by either the oxidized species of the redox mediator or the oxidized dye itself.

In solid-state DSSCs, the electrolyte in its solid state is the hole transporting material (HTM) or hole mediator. Dye regeneration is accomplished in solid-state DSSCs via the hole transfer from the oxidized state of the dye into the HOMO level of the HTM. The HTM is regenerated from the counter electrode by the charge transfer process.⁴⁵

The state of the gel electrolyte (GE) is between the liquid and solid electrolyte. In quasi-solid-state DSSCs, the GEs contain a significant amount of liquid electrolyte retained by gelating materials, such as polymers,¹⁹ inorganic nanofillers,⁴⁶ and nanocomposite polymers.⁴⁷

3.2. Ion Transport in the Redox Electrolytes. Generally, the performance of electrolytes is evaluated by their ion transportability. Ionic conductivity is due to the movement of ionic charges. The ionic conductivity (σ) of any electrolyte (eq 12) is the product of the charge, concentration, and mobility of the carrier ions^{48–50}

$$\sigma = \sum q_i \mu_i C_i \quad (12)$$

where μ_i , q_i , and C_i are the mobility, charge, and concentration of the ionic specimen, i , respectively.

The mobility of the carrier ion is related to the diffusion coefficient (D_i) of the carrier ion by the Einstein kinetic theory through eq 13

$$\mu_i = \frac{q_i}{kT} D_i \quad (13)$$

The diffusion coefficient is related to the viscosity of the medium by the Stokes–Einstein equation (eq 14)

$$D_i = \frac{kT}{6\pi\eta r_i} \quad (14)$$

where k is the Boltzmann constant, η is the viscosity of the medium, r is the radius of the ion, and T is the absolute temperature.

Therefore, the diffusion coefficient is inversely proportional to the viscosity of the medium (eq 3).

The general relationship between ionic conductivity and diffusion can be obtained from eq 15:

$$\sigma = \sum \frac{q_i^2 C_i}{kT} D_i \quad (15)$$

Therefore, with increasing diffusion of carrier ions in the electrolyte medium, the ionic conductivity increases, and with decreasing diffusion, the ionic conductivity decreases.

The concentration and mobility of carrier ions are thermally activated. The temperature dependence on the ionic conductivity or diffusion coefficient can be explained from the Arrhenius equation^{51,52}

$$\sigma(T) = \sigma_0 \exp\left(\frac{-E_a}{kT}\right) \quad (16)$$

where σ_0 is the pre-exponential factor linked to the concentration of the carrier ions, E_a is the activation energy, k is the Boltzmann constant, and T is the absolute temperature.

The activation energy (E_a) of the electrolyte can be obtained from the slope of the $\log(\sigma(T))$ versus $1/T$ plot (see eq 16). The low activation energy of the electrolytes indicates that less energy is required by the carrier ions to initiate the migration process.

The Arrhenius equation explains the behavior of the ionic conductivity with temperature for homogeneous electrolytes very well. Usually, in all cases of LEs and most cases of GEs, the temperature-dependent ionic conductivity fits the Arrhenius equation well; however, the deviation from the Arrhenius behavior is observed for full-solid polymer electrolytes and some cases of GE.⁵³

For nonhomogeneous electrolytes such as solid polymer electrolytes, the Vogel–Tammann–Fulcher (VTF) equation^{54–56} is generally used to clarify the conductivity behavior of the electrolytes with temperature (eq 17)

$$\sigma(T) = \sigma_0 \exp\left(\frac{-B}{k(T - T_0)}\right) = \sigma_0 T^{-1/2} \exp\left(\frac{-E_a}{k(T - T_0)}\right) \quad (17)$$

where B is the pseudo activation energy linked to the configuration entropy of the polymer chain and T_0 is the equilibrium transition temperature (usually $T_0 \approx T_g - 50$ K).

The Dahms–Ruff equation (eq 18) can be utilized to explain the apparent diffusion coefficient for the concentrated system.^{57,58}

$$D_{\text{app}} = D_{\text{phys}} + D_{\text{ex}} = D_{\text{phys}} + k_{\text{ex}} \delta^2 c / 6 \quad (18)$$

D_{phys} is the viscosity dependent physical diffusion coefficient, which is related to the Stokes–Einstein equation (see eq 14). D_{ex} is the electron exchange diffusion coefficient by the electron hopping process, which is related to the rate constant (k_{ex}) for electron exchange, concentration (c) of the redox species, and average center-to-center distance (δ) between the redox species.⁵⁹ The nondiffusional hopping (e.g., Grotthus-like exchange) mechanism of triiodide (see eq 26) can be rationalized by the electron exchange diffusion coefficient (D_{ex}).

3.2.1. Measurement of Ionic Conductivity from Bulk Resistance. Generally, the ionic conductivity of the electrolytes is obtained by estimating the bulk resistance of the electrolytes (R_b) in the Nyquist plot (also known as the Cole–Cole plot) using eq 19

$$\sigma = \frac{l}{R_b A} \quad (19)$$

where l is the electrolyte thickness, A is the electrolyte area, and R_b is the bulk resistance of the electrolyte obtained from the impedance. The Nyquist plot is obtained from the impedance measurement of the electrolyte-blocking electrode cell, placing or sandwiching electrolytes between two inert electrodes (usually stainless-steel electrodes).

To regenerate dye and electrolyte during operation of DSSCs under 1 sun, the ionic conductivity should be $\geq 10^{-3}$ S cm^{-1} . However, the threshold value of ionic conductivity may vary with the light illumination, redox shuttle, additive, and medium of the electrolytes.

3.2.2. Evaluation of Charge Transfer Resistances by Impedance. To evaluate charge transfer resistance between electrodes and electrolytes, electrochemical impedance spectroscopy (EIS) was performed with a symmetrical dummy cell (counter electrode/electrolytes/counter electrode). In the Nyquist plot, two semicircles are found; the intercept in the real axis of the high-frequency region is regarded as the series resistance (R_s), the left semicircle is due to the charge transfer resistance (R_{ct}) at the electrode–electrolyte interface, and the right semicircle arises due to the Nernst diffusion impedance (Z_n) of the redox shuttle in the electrolytes (see Figure 4a).⁶⁰

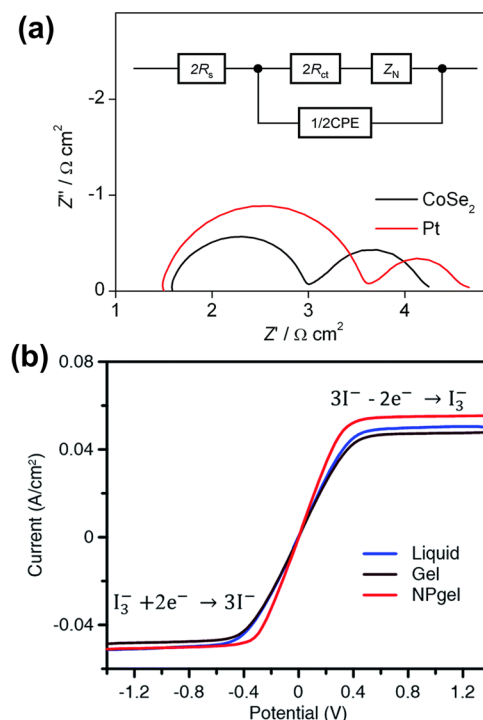
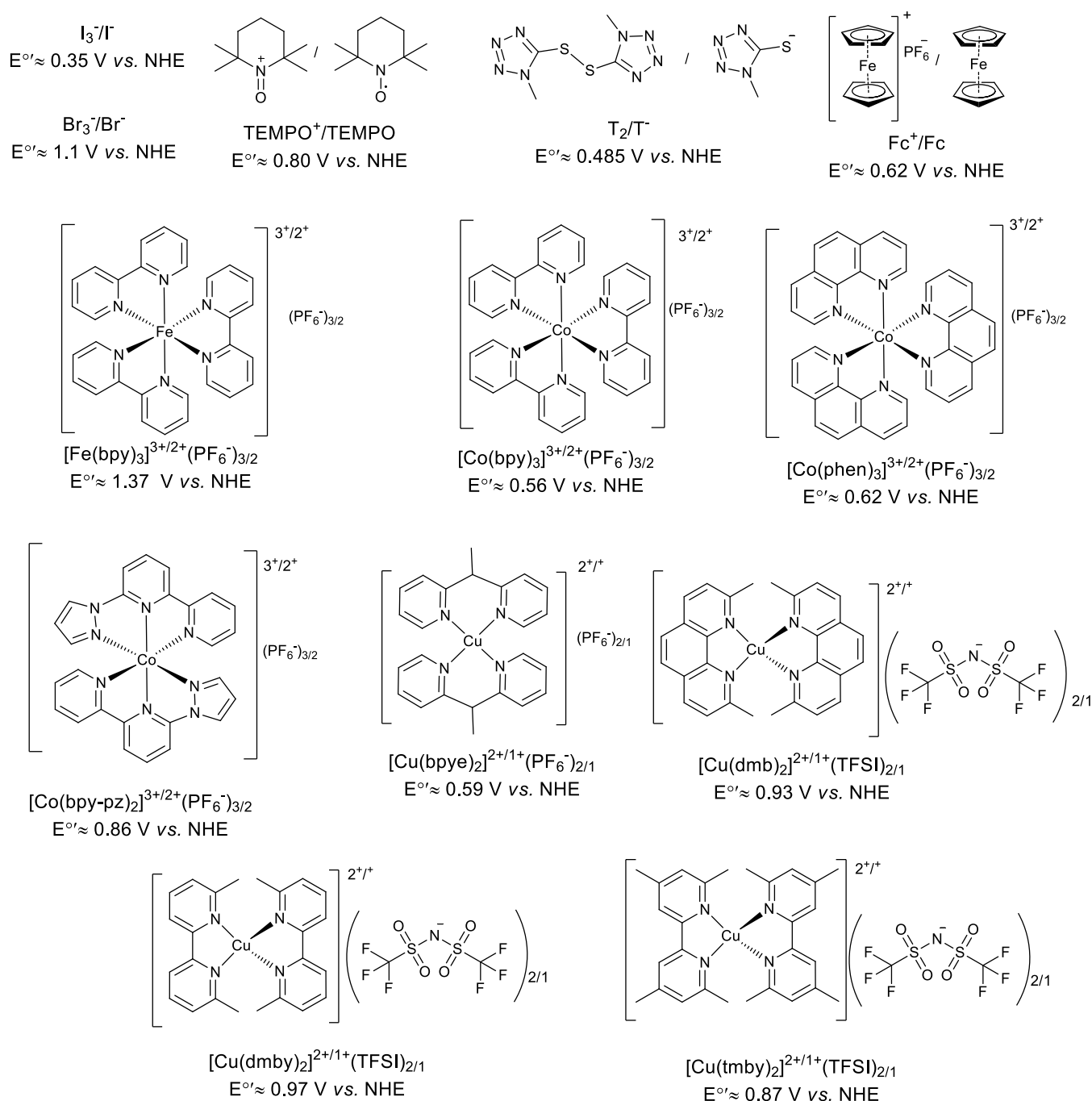


Figure 4. (a) Charge transfer resistance of electrode/electrolytes determined from Nyquist plots in EIS measurement of a symmetrical dummy cell. Reprinted with permission from ref 60. Copyright 2014 Royal Society of Chemistry. (b) Apparent diffusion of I_3^- determined from the cathodic limiting current of J - V curves in LSV measurements (scan rate 10 mV s^{-1}) of a symmetrical dummy cell. Reprinted with permission from ref 62. Copyright 2017 Royal Society of Chemistry.

3.2.3. Measurement of Apparent Diffusion Coefficient from Steady-State Limiting Current. Usually, the diffusion-limited current density (J_{lim}) can be obtained by measuring the cyclic voltammetry (CV) or linear sweep voltammetry (LSV) of a symmetrical dummy cell, counter electrode/electrolytes/counter electrode. In the case of CV, a slow scan rate (usually

Scheme 1. Structures of Some Important Redox Couples (R⁺/R) Used in DSSC Electrolytes as Redox Mediators and Their Standard Redox Potentials


5–10 mV s⁻¹) is required to obtain steady-state conditions.⁶¹ The diffusion-limited current density is related to the apparent diffusion coefficient (D_{app}) of the redox species of electrolytes by eq 20

$$D_{app} = \frac{d}{2nFC_0} J_{lim} \quad (20)$$

where d is the electrolyte thickness, F is the Faraday constant, C_0 is the concentration of the redox species, and n is the number of electrons transferred for this process.

In LSV measurements (see Figure 4b),⁶² the anodic steady-state limiting current (upper plateau) is due to the electrochemical oxidation of the reduced species (I^-), and the

cathodic steady-state limiting current (lower plateau) is due to the electrochemical reduction of the oxidized species (I_3^-) in the electrolytes. Usually, due to the presence of excess I^- ions in the electrolytes, I_3^- is the limiting ion. Under steady-state conditions, both the anodic and cathodic current plateaus are usually similar. Therefore, the obtained limited current from LSV is mainly valid for the calculation of the apparent diffusion of I_3^- .^{63,64} For efficient operation of the DSSC under 1 sun, the apparent diffusion coefficient should be $\geq 10^{-6} \text{ cm}^2 \text{ s}^{-1}$.⁶¹

Fast dye generation and rapid diffusion minimize the recombination reaction (dark reaction) significantly; as a result, higher J_{sc} and V_{oc} values can be obtained by the device.

4. REDOX ELECTROLYTE COMPONENTS

4.1. Redox Shuttles. In DSSCs, the redox couple is used in liquid or gel electrolytes as a redox mediator or the redox shuttle and the HTM is used in solid electrolytes as a hole mediator. The role of the redox shuttle is to regenerate the dye by giving electrons to the photo-oxidized dye and transferring the electrons from the counter electrode to the oxidized dye to complete the circuit. The redox shuttle is the crucial part of the DSSC that strongly influences the photovoltage of the device. The redox shuttle sets the electrochemical potential at the counter electrode and influences the electrochemical potential of the TiO₂ working electrode through the recombination of electrons in the TiO₂ by their oxidized species.⁶⁵ Under light illumination, the maximum theoretical V_{oc} for the DSSC can be estimated from the difference between the quasi-Fermi level of electrons in the TiO₂ semiconductor, which approaches the energy level of the TiO₂ conduction band edge under intense light illumination, and the redox potential of the redox shuttle (see eq 11).

The redox potential of the electrolyte system can be obtained by the Nernst equation (eq 21)

$$E_{\text{redox}} = E^{o'} + \frac{RT}{nF} \ln \frac{[\text{Ox}]}{[\text{Red}]} \quad (21)$$

where $E^{o'}$ is the formal potential, R is the ideal gas constant, F is the Faraday constant, T is the absolute temperature, n is the number of electron transfers for the redox reaction (for I^-/I_3^- , $n = 2$; for $\text{Co}^{2+}/\text{Co}^{3+}$ (complex) and $\text{Cu}^+/\text{Cu}^{2+}$ (complex), $n = 1$), and $[\text{Ox}]$ and $[\text{Red}]$ are the concentrations of oxidized and reduced species, respectively.

From the discovery of the DSSC up to now, I_3^-/I^- ,^{66–72} $\text{Br}_3^-/\text{Br}^-$,^{73,74} pseudohalogens such as $\text{Se}(\text{CN})_3^-/\text{Se}(\text{CN})_3^-$ and $(\text{SCN})_3^-/\text{SCN}^-$,⁷⁶ various transition-metal complexes such as $\text{Co}^{3+}/\text{Co}^{2+}$ (complex),^{4,15,77–80} $\text{Cu}^{2+}/\text{Cu}^+$ (complex),^{8,12,14,16,81–83} $\text{Fe}^{3+}/\text{Fe}^{2+}$ (complex),^{84,85} and ferrocenium/ferrocene (Fc^+/Fc),^{13,86} and organic redox shuttles such as $\text{TEMPO}^+/\text{TEMPO}$ (2,2,6,6-tetramethyl-1-piperidinyloxy radical)⁸⁷ and T_2 (dimer of *S*-mercapto-1-methyltetrazole ion)/ T^- (*S*-mercapto-1-methyltetrazole ion)⁸⁸ have been employed and studied as redox shuttles in DSSC electrolytes. Standard redox potentials of some redox shuttles used in DSSCs are shown in Scheme 1.

A redox couple with a higher redox potential may result in a high photovoltage of the device. To preserve the photocurrent, the dye regeneration by the redox mediator should be faster than the electron back transfer from the TiO₂ to the oxidized dye.¹⁶ A sufficient driving force for dye regeneration is required to avoid the recombination of injected electrons with the oxidized dye. An inadequate driving force for dye regeneration can cause a lower photovoltaic performance by reducing the short-circuit current density (J_{sc}) and V_{oc} because of the recombination of injected electrons with the photo-oxidized dye. The high driving force for dye regeneration can also limit the V_{oc} of the cell. Hence, an optimum driving force (around 20–25 kJ mol⁻¹) is required for efficient dye regeneration; this is possible by selecting a suitable redox couple for the specific dye.^{89,90}

Therefore, novel redox mediators with a more positive redox potential that maintain the optimum driving force for dye regeneration are the key to enhancing the open-circuit potential and photocurrent of the device. Hence, the general strategy for the V_{oc} enhancement of a device is to

simultaneously lower both the HOMO level of the dye and the reduction potential of the redox shuttle toward a positive potential (see Figure 5). The optimum driving force for dye regeneration can be varied with different redox couples.

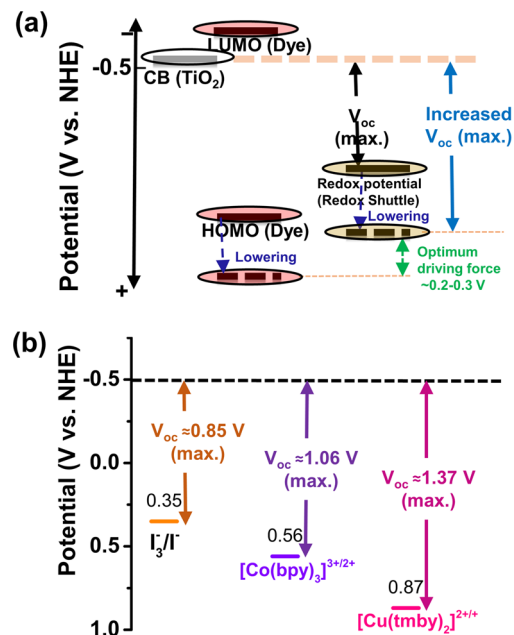


Figure 5. (a) Strategy for enhancing the maximum theoretical photovoltage (V_{oc}) by simultaneously lowering the redox shuttle redox potential and the ground-state oxidation potential of the dye toward a more positive potential to ensure the optimum driving force for fast dye regeneration. (b) Comparison of the redox potentials and possible maximum open-circuit voltages among three of the most efficient redox couples used in the DSSC.

4.1.1. Halogenide Redox Shuttles. The I_3^-/I^- redox shuttle shows an impressive performance in DSSCs and has been commonly used in the DSSC redox electrolytes since its invention. The standard redox potential of the I_3^-/I^- redox couple is around 0.35 V (vs the normal hydrogen electrode (NHE));⁶⁵ thus, there is a mismatch of more than 0.65 V with dyes having an oxidation potential above 1.0 V. This high driving force (>0.65 V) for the reduction of the oxidized dye allows for a rapid dye regeneration and slow recombination of injected electrons in TiO₂ with I_3^- , which favor the high J_{sc} value of the device. However, the excess driving force for dye regeneration permits a significant V_{oc} loss above 0.65 V for the I_3^-/I^- electrolyte-based device.^{44,65} Furthermore, dye regeneration by I_3^-/I^- electrolytes involves complex two-electron redox chemistry (eqs 22–24).⁶⁵



The intermediate $\text{I}_2^{\bullet -}$ radical species formed in the dye regeneration process has a more negative redox potential than the standard redox potential of the I_3^-/I^- redox species. Thus, the formation of intermediate radical species causes additional potential loss. Light absorption in the blue region of the visible spectrum by the I_3^-/I^- redox electrolytes⁹¹ competes with the dye light absorption and causes a lower photocurrent. In

addition, corrosiveness with the metal current collector, especially the Ag metal grid, by the I_3^-/I^- redox electrolytes limits the commercial scale-up of the DSSC to a module.^{88,92} A study of various metal thin films with I_3^-/I^- redox electrolytes by Okada et al. confirms that Ag, Au, and Al are highly corrosive with I_3^-/I^- , while Pt, Ti, and Ni are less corrosive.⁹² Therefore, competitive visible light absorption, corrosion with metals, and limitation of the photovoltage are the major drawbacks of the I_3^-/I^- redox couple. To overcome these limitations, a suitable alternative to the I_3^-/I^- redox couple is needed.

The Br_3^-/Br^- redox couple was also applied in the DSSC because of its higher positive reduction potential (~ 1.1 V vs NHE) than the I_3^-/I^- redox shuttle (~ 0.35 V vs NHE).^{65,73,93} However, the Br_3^-/Br^- redox electrolyte enhances the V_{oc} up to 1 V for the carbazole dye⁷⁴ but reduces J_{sc} . The dye regeneration by Br^- is much slower than that of I^- due to the low driving forces with most of the dyes. Besides, the Br_3^-/Br^- redox couple has a problem similar to that of I_3^-/I^- , including environmental impact.

A comparison study of pseudohalide redox couples and I_3^-/I^- redox couples with the N3-dye was carried out by Oskam et al.⁷⁶ They discovered that $Se(CN)_3^-/Se(CN)^-$ and I_3^-/I^- -based devices had similar V_{oc} values. However, a significant decrease in J_{sc} for the $Se(CN)_3^-/Se(CN)^-$ redox couple based device was observed. The J_{sc} and V_{oc} values were both the lowest for the $(SCN)_3^-/SCN^-$ -based device.⁷⁶ Despite the more positive equilibrium potentials of pseudohalide redox couples than the I_3^-/I^- redox couple, the V_{oc} value did not improve.⁷⁶ Therefore, a more positive equilibrium potential is not always applicable to account for the V_{oc} enhancement of the device. Shifting of the FTO/dye-sensitized TiO_2 and FTO/Pt electrode potential with the equilibrium potential of the redox couple is also required to account for the deviation of the V_{oc} value. By transient absorbance studies, Oskam et al. concluded that dye regeneration is much slower for the $Se(CN)_3^-/Se(CN)^-$ and $(SCN)_3^-/SCN^-$ redox couples than the I_3^-/I^- redox couple, and the decreasing order of dye-regeneration rate is as follows: $I_3^-/I^- > Se(CN)_3^-/Se(CN)^- > (SCN)_3^-/SCN^-$.⁷⁶

4.1.2. Organic Redox Shuttles. The stable organic radical 2,2,6,6-tetramethyl-1-piperidinyloxy (TEMPO) and its ion $TEMPO^+$ can also be used as redox mediators in DSSC electrolytes. The standard redox potential of $TEMPO^+/TEMPO$ (0.80 V vs NHE) is higher than that of the I_3^-/I^- redox couple (0.35 V vs NHE). Zhang et al. reported a 5.4% power conversion efficiency under 1-sun conditions with a high photovoltage of 830 mV.⁸⁷ However, the $TEMPO^+/TEMPO$ redox couple based device suffers from a low J_{sc} value due to the fast recombination (back electron transfer from TiO_2). The long-term stability of the $TEMPO^+/TEMPO$ redox electrolyte based device also needs to be improved. Another iodine-free redox couple, 5-mercapto-1-methyltetrazole ion (T^-) and its dimer (T_2), was also used in DSSC electrolytes by Wang et al. due to advantages like noncorrosiveness, negligible visible light absorption, and a closer redox potential (~ 0.48 V vs NHE) with the I_3^-/I^- redox couple. Wang et al. achieved a competitive power conversion efficiency of 6.4% under 1 sun illumination with J_{sc} of 16.18 mA cm^{-2} , V_{oc} of 681 mV, and FF of 0.58 using a Ru-based Z907Na dye.⁸⁸ Despite the promising performances of the T_2/T^- redox couple, the long-term stability of the device still needs to be improved. A thiol-based self-assembled layer may form on the metal counter electrode,

and devices with the T_2/T^- redox couple and the Pt counter electrode suffer from stability problems.⁴⁴

4.1.3. Transition-Metal Complexes for Redox Shuttles. The ferrocenium hexafluorophosphate/ferrocene (Fc^+/Fc) redox couple can be an alternative redox couple because of its noncorrosive nature, simple one-electron-transfer redox reaction chemistry, abundance, and suitable redox potential (0.62 V vs NHE).^{13,94} The redox potential of Fc^+/Fc can be further tuned by introducing various substituents in the cyclopentadienyl ring. Various substituted Fc compounds are also commercially available.^{95,96} Daeneke et al. reported a 7.5% efficiency under 1-sun condition by using the Fc^+/Fc redox couple and an organic sensitizer with the coadsorbent chenodeoxycholic acid (CDCA). A V_{oc} enhancement of about 100 mV compared to I_3^-/I^- was observed for the Fc^+/Fc -based device due to the more positive redox potential of the Fc^+/Fc redox couple.¹³ However, the charge recombination rate is faster for Fc^+/Fc redox electrolytes than for the I_3^-/I^- redox couple, which causes a reduction in the J_{sc} value for the Fc^+/Fc -based device. Furthermore, an oxygen-free environment is required for both the electrolyte preparation and cell fabrication due to the instability of the Fc^+ in the presence of O_2 . The $Fe(bpy)_3^{3+/2+}$ redox couple can also be interesting due to its positive redox potential of around 1.37 V (vs NHE). However, a proper dye with a more positive oxidation potential is required for these redox electrolytes. Rodrigues et al. obtained a 1.4 V photovoltage by using $Fe(bpy)_3^{3+/2+}$ redox electrolytes with the modified D- π -A structure based organic sensitizer RR9. However, the efficiency of the device was poor due to the very low J_{sc} value and fill factor.⁹⁷ The stability of the Fe^{3+}/Fe^{2+} electrolyte based device was also not reported.^{84,85,97} Ni- and Mn-based complexes were also utilized as redox shuttles for DSSCs; however, their photovoltaic performances were not significantly improved.^{98,99} The greatest advantage of transition-metal complexes as redox mediators is that the redox potential of the complexes and V_{oc} of the device can be tuned by varying ligands of the complexes.

Among the various transition-metal complexes, cobalt complexes have received more attention as redox mediators in the DSSC. Negligible visible light absorption, less corrosiveness toward metals, outer-sphere one-electron-redox chemistry, and higher positive redox potential of cobalt polypyridine complexes make cobalt complexes promising as redox shuttles. Generally, the Co(II) complex exists in the high-spin (HS) state at room temperature, as a quartet state, while the Co(III) complex is in a low-spin (LS) state, as a triplet state (see Figure 6).¹⁰⁰ The large reorganization energy between d^7 (HS) and d^6 (LS) causes slow regeneration of Co(II) species in the counter electrode and enhanced charge recombination with Co(III) species. Slow mass transfer due to the large molecular size,^{101,102} rapid back electron transfer from TiO_2 to Co^{3+} species,¹⁰³ and slow regeneration of Co^{2+}

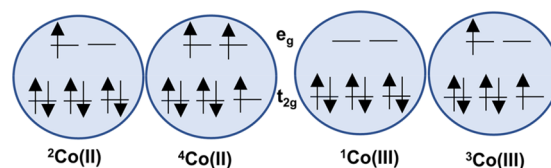


Figure 6. Electronic configurations of Co(II) species in doublet and quartet states and Co(III) species in singlet and triplet states.

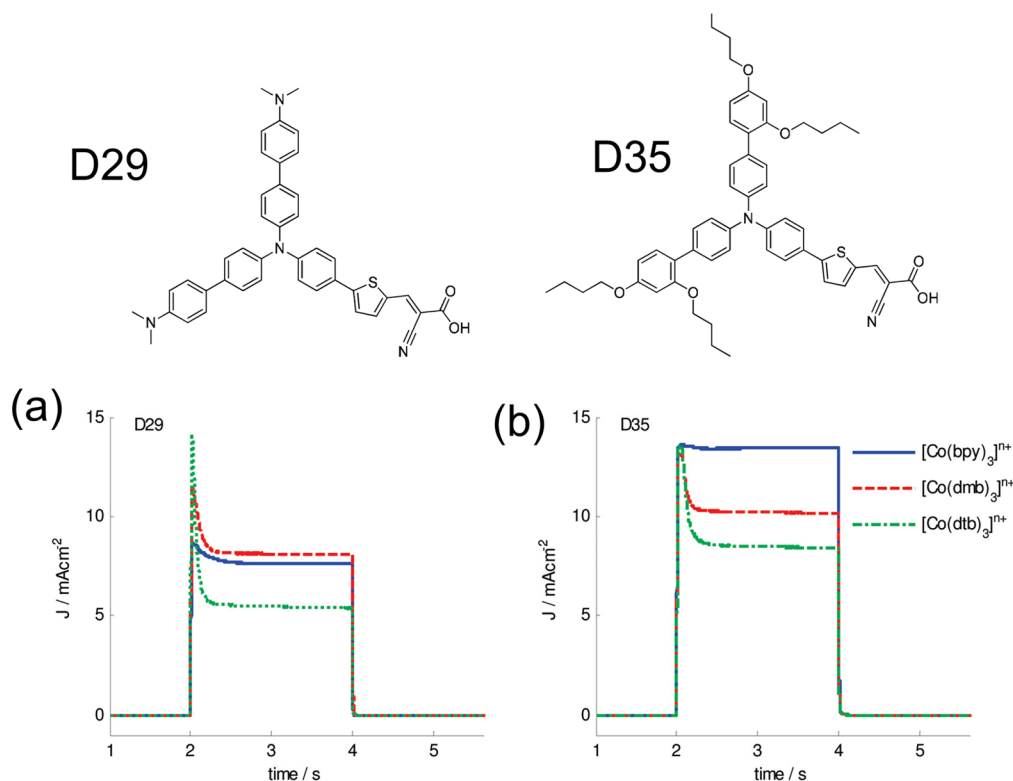


Figure 7. Chemical structure of dyes and plots of current transients for various Co complexes with two different dyes: (a) D29; (b) D35. Mass transport can be avoided by using a less bulky $\text{Co}(\text{bpy})_2$ complex redox shuttle with the sterically bulky D35 dye. Reprinted with permission from ref 15. Copyright 2010 American Chemical Society.

species in the Pt counter electrode¹⁰³ are the major challenges of the cobalt complexes; these can be overcome by enhancing the solubility of the complex by introducing a suitable substituent in the ligand, optimizing the device structure (especially the TiO_2 film thickness), reducing the spacer thickness between electrodes, introducing a passivation layer to inhibit the back transfer reaction, and using a suitable catalyst in the counter electrode.

The redox potential of the cobalt complexes can be tuned by using an appropriate ligand to match the oxidation potential of the dye. Feldt et al. tested a series of cobalt complexes with different redox potentials as a one-electron outer-sphere redox mediator in the DSSC.¹⁵ The standard redox potentials of cobalt(III/II) tris(2,2'-bipyridine), $[\text{Co}(\text{bpy})_3]^{3+/2+}$, cobalt(III/II) tris(4,4'-dimethyl-2,2'-bipyridine), $[\text{Co}(\text{dmb})_3]^{3+/2+}$, cobalt(III/II) tris(4,4'-di-*tert*-butyl-2,2'-bipyridine), $[\text{Co}(\text{dtb})_3]^{3+/2+}$, and cobalt(III/II) tris(1,10-phenanthroline), $[\text{Co}(\text{phen})_3]^{3+/2+}$, were 0.56, 0.43, 0.43, and 0.62 V, respectively. Here, for all the complexes, the counterion was hexafluorophosphate (PF_6^-). The V_{oc} value of the devices should increase with increasing redox potential of the cobalt complexes; however, Feldt et al. obtained an optimum V_{oc} and J_{sc} from the $[\text{Co}(\text{bpy})_3]^{3+/2+}$ redox couple due to the optimum driving force for dye regeneration, less mass transport limitation due to the less bulky $[\text{Cu}(\text{bpy})_3]$ complexes (see Figure 7), and reduction of recombination due to the introduction of steric bulk in the D35 dye.¹⁵

The standard redox potential of the cobalt complex $[\text{Co}(\text{bpy})_3]^{3+/2+}(\text{B}(\text{CN})_4)^{-3/2}$ redox couple is 0.57 V (vs NHE).⁷⁹ Here, 2,2'-bipyridine (bpy) is the bidentate ligand and tetracyanoborate ($\text{B}(\text{CN})_4^-$) is the counterion of the cobalt complex. By a combination of the $[\text{Co}(\text{bpy})_3]^{3+/2+}(\text{B}(\text{CN})_4)^{-3/2}$ redox couple as the redox mediator and the donor- π -bridge-acceptor (D- π -A) structure-based Zn porphyrin dye YD2-o-C8 as a sensitizer, Yella et al. achieved a 11.9% efficiency with a V_{oc} of 965 mV, J_{sc} of 17.3 mA cm^{-2} , and FF of 0.71.⁷⁹ By cosensitization with the organic dye, they further increased the efficiency to 12.5% under simulated 1-sun (AM 1.5G) illumination. The presence of octyloxy groups in the Zn porphyrin YD2-o-C8 sensitizer enables slower recombination of the injected electron in TiO_2 with $\text{Co}^{3+}(\text{bpy})_3$. This dye also absorbs light across the entire visible range.⁷⁹ Kang et al. obtained a 12.1% efficiency under 1-sun illumination by using the D- π -A structured Zn-porphyrin SGT-021 dye with the cobalt complex redox shuttle $[\text{Co}(\text{bpy})_3]^{3+/2+}(\text{B}(\text{CN})_4)^{-3/2}$. In this case, the presence of the octyloxy group in the dye structure also prevented the electron back transfer recombination reaction and retained a V_{oc} close to 1 V without sacrificing the J_{sc} value.⁴ The D- π -A structure based Zn-porphyrin SGT-025 also gave a promising efficiency of up to 11.0%⁷⁷ with a coadsorbent π -conjugated phenyl linker (HC-A1).¹⁰⁴ Therefore, the D- π -A structure based Zn-porphyrin sensitizer is a promising dye for cobalt complex redox electrolytes.

The standard redox potential of the tridentate ligand bpy-pz (6-(1H-pyrazol-1-yl)-2,2'-bipyridine) containing the $[\text{Co}(\text{bpy-pz})_2]^{3+/2+}(\text{PF}_6^-)_{3/2}$ redox couple is 0.86 V (vs NHE), which is higher than the standard redox potential of the bidentate 2,2'-bipyridine ligand based $[\text{Co}(\text{bpy})_3]^{3+/2+}(\text{PF}_6^-)_{3/2}$ redox couple (~ 0.56 V vs NHE). Thus, the presence of pyrazole in the ligand bpy-pz stabilizes the HOMO level of the complexes more than does 2,2'-bipyridine (bpy). By using the Y123 organic sensitizer and $[\text{Co}(\text{bpy-pz})_2]^{3+/2+}(\text{PF}_6^-)_{3/2}$ redox electrolyte, Yum et al. achieved a 10% efficiency with a V_{oc}

The standard redox potential of the tridentate ligand bpy-pz (6-(1H-pyrazol-1-yl)-2,2'-bipyridine) containing the $[\text{Co}(\text{bpy-pz})_2]^{3+/2+}(\text{PF}_6^-)_{3/2}$ redox couple is 0.86 V (vs NHE), which is higher than the standard redox potential of the bidentate 2,2'-bipyridine ligand based $[\text{Co}(\text{bpy})_3]^{3+/2+}(\text{PF}_6^-)_{3/2}$ redox couple (~ 0.56 V vs NHE). Thus, the presence of pyrazole in the ligand bpy-pz stabilizes the HOMO level of the complexes more than does 2,2'-bipyridine (bpy). By using the Y123 organic sensitizer and $[\text{Co}(\text{bpy-pz})_2]^{3+/2+}(\text{PF}_6^-)_{3/2}$ redox electrolyte, Yum et al. achieved a 10% efficiency with a V_{oc}

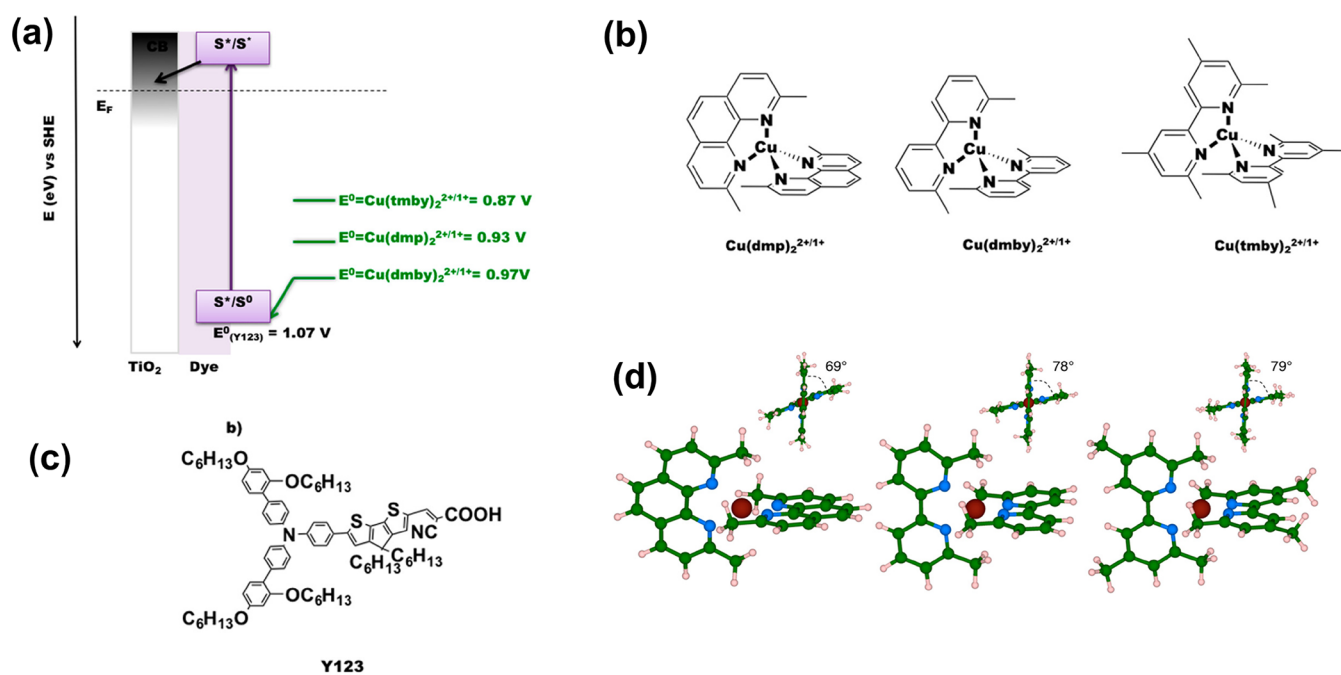


Figure 8. (a) Energy levels in DSSC for Y123 dye and Cu complexes, the chemical structures of (b) various Cu complexes and (c) Y123 dye, and (d) the minimum-energy structures of Cu(II) complexes. Reprinted with permission from ref 16. Copyright 2016 American Chemical Society.

above 1 V.⁷⁸ In 2014, Mathew et al. reported a DSSC with a 13.0% efficiency using a D- π -A structured porphyrin dye, SM315, with the [Co(bpy)₃]^{3+/2+} redox mediator.¹⁰⁵ In 2015, Kakiage et al. reported a record efficiency of 14.3% under full sun illumination using a cosensitized organic dye, ADEKA-1 + LEG4, with the [Co(phen)₃]^{3+/2+} redox couple.¹¹ In 2018, Ren et al. reported a remarkable efficiency of 12.6% under full sun (AM 1.5G) illumination using the [Co(bpy)₃]^{3+/2+} redox mediator and the D- π -A structured organic blue dye R6.⁸⁰ Ji et al. reported an outstanding efficiency of 14.2% under 1-sun (AM 1.5G illumination) conditions by using the [Co(bpy)₃]^{3+/2+} complex as the redox mediator and a cosensitized D- π -A structured organic dye, SGT-149, and a porphyrin dye, SGT-021, with the coadsorbent HC-A1.⁹

The driving force for the dye regeneration is sufficient for the [Co(phen)₃]^{3+/2+}(PF₆⁻)_{3/2} and [Co(bpy)₃]^{3+/2+}(PF₆⁻)_{3/2} complexes due to the moderate positive redox potential. Therefore, when [Co(phen)₃]^{3+/2+} and [Co(bpy)₃]^{3+/2+} complexes are used as redox mediators, a photovoltage of around 1 V should be obtained from the device if the recombination reaction can be minimized by optimizing the device and selecting the proper sensitizer. For efficient dye regeneration, a large driving force is usually required for the cobalt complexes due to the high reorganization energy between high-spin d⁷ states of Co(II) and low-spin d⁶ states of Co(III)-complexes,^{100,106} which is the major drawback of the Co complexes.

Copper complexes have received a great deal of attention as redox mediators due to their fast electron self-exchange property, which decreases the charge transport limitation.^{14,82} Copper complexes have been used both in liquid electrolytes as redox mediators and also in solid electrolytes as hole mediators.^{8,107} Like other transition-metal complexes, the redox potential of the copper complexes can also be tuned by changing the ligands in the complex. In addition, copper is nontoxic, abundant in the Earth, and comparatively cheaper

than cobalt. In 2005, Hattori et al. first introduced various blue copper complexes as redox mediators in the DSSC. However, the efficiency of the device was poor at that time, but the V_{oc} of the device using [Cu(dmp)₂]^{2+/+} as the redox mediator was higher than the V_{oc} of the device using the I³⁻/I⁻ redox mediator due to the more positive standard redox potential of [Cu(dmp)₂]^{2+/+} (0.93 vs NHE).¹⁴ In 2011, Bai et al. reported a C218 dye sensitized solar cell with 7.0% efficiency using [Cu(dmp)₂]^{2+/+} complex redox shuttles.⁸³ The enhancement in the efficiency of the copper complex redox couple based device was mainly due to the significant increase in the V_{oc} (0.93 V) because of the higher positive redox potential of the copper complexes. The J_{sc} value for the copper electrolyte was lower than that for the iodine electrolyte. They also found a lower IPCE, especially in the blue region, for the copper electrolyte device than for the iodine electrolyte device. Their IPCE data indicate the stronger absorption of copper complexes than iodine electrolytes. They also reported that the copper redox shuttles may transfer electrons to a lesser extent to a noble metal, carbon black, and conducting oxides, which causes the poor fill factor. Therefore, careful selection of counter electrodes, copper complexes, and photosensitizers can further improve the efficiency of the device. Cong et al. compared the [Cu(bpye)₂]^{2+/+} redox shuttle with the [Co(bpy)₃]^{3+/2+} redox couple and found a higher PCE as well as a higher V_{oc} for the [Cu(bpye)₂]^{2+/+} redox couple based device than the [Co(bpy)₃]^{3+/2+} redox couple based device due to the more positive redox potential (~0.59 V) of [Cu(bpye)₂]^{2+/+} complexes.⁸² The main disadvantage of the [Co(bpy)₃]^{3+/2+} redox shuttle is the mass transport problem, which may be possible to overcome by changing the ligand of Co complexes to bpye. Pradhan et al. found in their study with different redox electrolytes that the [Cu(dmb)]^{2+/+} redox shuttle showed a lower mass transport, better diffusion, and comparatively low driving force (~0.1 V) required for efficient dye regeneration compared to the [Co(bpy)₃]^{3+/2+} redox shuttles.¹⁰⁸ Saygili et al.

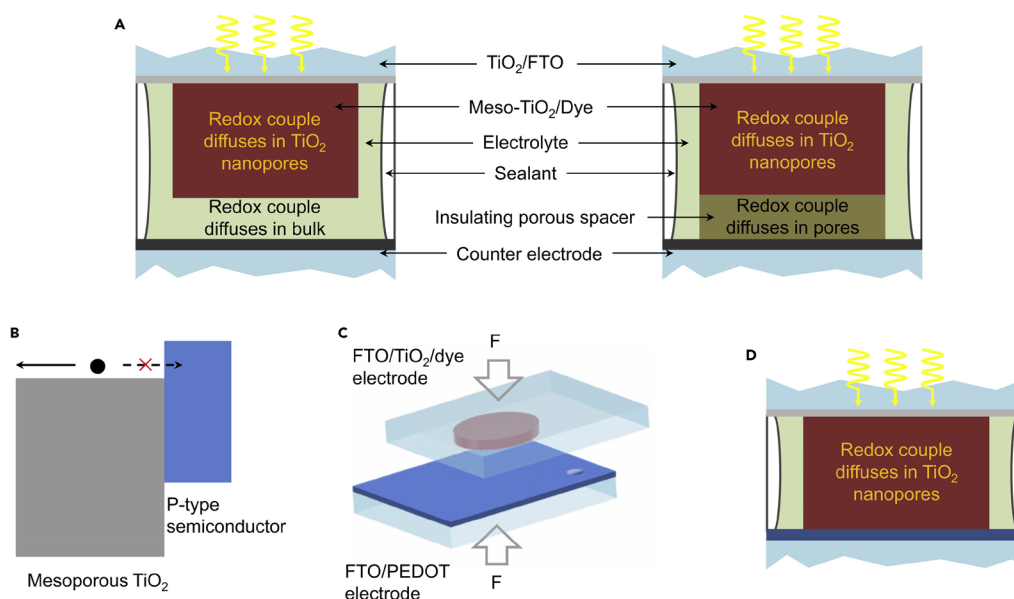


Figure 9. Modification of DSSC device structure by direct contact between the dye-sensitized TiO₂ photoanode and the electrically deposited poly(3,4-ethylenedioxythiophene) (PEDOT) in the FTO. Reprinted with permission from ref 12. Copyright 2018 Elsevier.

reported DSSCs with over 10% efficiency using three different copper complexes, [Cu(dmp)₂]^{2+/+}TFSI_{2/1}, [Cu(dmby)₂]^{2+/+}TFSI_{2/1}, and [Cu(tmby)₂]^{2+/+}TFSI_{2/1}, as redox shuttles. The standard redox potential for [Cu(dmby)₂]^{2+/+}TFSI_{2/1} is 0.97 V (vs NHE), which is higher than the standard redox potential of the [Cu(tmby)₂]^{2+/+}TFSI_{2/1} complex (0.87 V vs NHE).¹⁶ Therefore, the ligand 6,6'-dimethyl-2,2'-bipyridine (dmby) in copper complexes reduces the redox potential toward a more positive potential than the ligand 4,4',6,6'-tetramethyl-2,2'-bipyridine (tmby). However, the differences in the V_{oc} values for the devices with these three different copper complexes were insignificant (V_{oc} : 1.07 V for [Cu(dmby)₂]^{2+/+}, 1.04 V for [Cu(tmby)₂]^{2+/+}, and 1.06 V for [Cu(dmp)₂]^{2+/+}).¹⁶ If we consider the energy level of the TiO₂ conduction band edge of -0.5 V (vs NHE), then the maximum theoretical V_{oc} under an intense light condition for the device with the [Cu(tmby)₂]^{2+/+} complex redox mediator (redox potential of 0.87 V vs NHE) should be 1.37 V. For the devices with [Cu(dmby)₂]^{2+/+} and [Cu(dmp)₂]^{2+/+}, the maximum theoretical V_{oc} values can be 1.47 and 1.43 V, respectively (see Figure 8).

The theoretical losses of V_{oc} were around 400, 330, and 370 mV for the devices with [Cu(dmby)₂]^{2+/+}, [Cu(tmby)₂]^{2+/+}, and [Cu(dmp)₂]^{2+/+}, respectively. The lowest loss of V_{oc} was for the device with the [Cu(tmby)₂]^{2+/+} complex redox couple probably due to the slower back transfer recombination. There was an enhancement of the J_{sc} value for the device with the [Cu(tmby)₂]^{2+/+}TFSI_{2/1} redox couple. The small driving force is required to regenerate the dye efficiently by these Cu complexes due to the low reorganization energy, which may be attributed to the distorted-tetragonal structure of the copper(II) complexes (see Figure 8d) due to the steric hindrance of methyl groups in the 2,9-positions of the ligand.

Cao et al. reported an outstanding efficiency of 13.1% under standard AM 1.5G illumination for the [Cu(tmby)₂]^{2+/+} redox couple by modifying the device architecture by direct contact between the dye-sensitized TiO₂ photoanode and the electrically deposited poly(3,4-ethylenedioxythiophene) (PEDOT)/FTO counter electrode (see Figure 9).¹²

There was no V_{oc} drop due to the direct contact between the large-band-gap PEDOT conducting polymer (p-type) and TiO₂ (n-type); this indicates the insignificant electrical shunt between them. Cao et al. achieved this outstanding performance by improving the light-harvesting efficiency using cosensitization of two D- π -A structured organic dyes, Y123 and XY1b, with the coadsorbent CDCA. The fill factor (0.79) was also noticeably high for copper electrolytes due to the improvement in the mass transport by using a high concentration of the redox couple and no TiCl₄ post-treatment. In this direct contact device architecture, the redox shuttle diffuses through TiO₂ nanopores and the Warburg resistance is significantly reduced due to the decrease in the diffusion path.¹²

In 2020, Ren et al. reported a DSSC with 12.7% efficiency with the [Cu(tmby)₂]^{2+/+} redox electrolyte using the cosensitized organic blue dye R7 with the Y123 dye. In 2021, Zhang et al. introduced the Cu(tmby)^{2+/+} redox mediator in the D- π -A structure based organic dye MSS.⁸ They managed to maintain a theoretical V_{oc} loss of only 130 mV for the MSS dye, which may be due to the reduction of the back interfacial recombination and less driving force required for efficient dye regeneration by the Cu complexes. However, the J_{sc} value for the MSS-dye-based device was poor due to the low light-harvesting efficiency of that dye. By using the D- π -A structured organic dye XY1b with the adsorbent CDCA as a sensitizer and Cu(tmby)^{2+/+} complex as a redox mediator, they obtained an 11.8% efficiency under simulated 1-sun illumination with a comparatively high J_{sc} and fill factor. This may be due to the high LHE, efficient dye regeneration, and low back transfer recombination reaction. To further increase the LHE, they cosensitized the MSS dye with the XY1b dye and reported a remarkable efficiency of 13.5% under standard AM 1.5G (1-sun) illumination and 34.5% under 1000 lx illumination (Osram 930 warm white daylight).⁸ In 2022, Ren et al. reported a record PCE of 15.2% under 1-sun condition by using cosensitization with the newly developed SL9 and SL10 organic dyes with [Cu(tmby)₂]^{2+/+} redox electrolytes.²⁹ The device optimization by preabsorbing hydroxamic acid made it

possible to achieve such a high PCE of 15.2% of the cosensitized device. $[\text{Cu}(\text{tmby})]^{2+/+}$ complexes were also used as hole mediators in a complete solid-state DSSC, and a record efficiency of 11.0% was obtained by Cao et al.¹⁰⁷ Clearly, $\text{Cu}(\text{tmby})^{2+/+}$ complexes are more suitable as redox mediators due to several reasons: (1) the favorable redox potential (0.87 vs NHE) of $\text{Cu}(\text{tmby})^{2+/+}$ can minimize the photovoltage loss and a low driving force ($\sim 0.1\text{--}0.2$ V) is required for efficient dye regeneration due to the low internal reorganization energy of the complexes, (2) 6,6'-methyl substituents in the tmby ligand may protect copper complexes from oxidation and moisture,¹⁰⁷ and (3) the 6,6'-methyl substituent in tmby may be the reason for the rigid structure of the $\text{Cu}(\text{tmby})^{2+/+}$ complexes and prevent a structural change as much as possible, which may favor the rapid self-exchange electron transfer.^{107,109} It is observed that $\text{Co}^{3+/2+}$ and $\text{Cu}^{2+/+}$ complex redox electrolytes have already exceeded the performances of I_3^-/I^- redox electrolytes. Metal complex redox shuttles are more promising in terms of enhancing the V_{oc} of the device. In particular, $\text{Cu}(\text{tmby})_2^{2+/+}$ complexes are more suitable due to the low driving force required for efficient dye regeneration and minimal sacrifice of the J_{sc} value of the device. Judicious device optimization can play a key role in reducing the limitation of metal complex redox shuttles.

Both cobalt- and copper-based complexes can be potential redox shuttles for DSSCs by proper optimization of the electrolytes, tuning the redox potential by varying ligands to get an optimum driving force ($\sim 0.2\text{--}0.3$ V) for dye regeneration, using complexes with small reorganization energy between two states, optimization of the device to avoid charge recombination, and use of a suitable counter electrode for the specific redox shuttle.

4.1.4. Tandem or Mixed Redox Shuttles. Considering the synergistic effect of the mixed shuttles on the device performance, tandem or mixed redox shuttles, such as Co-complex-phenothiazine (PTZ)/Fc,¹¹⁰ sulfide/polysulfide-iodide,¹¹¹ TEMPO-iodide,¹¹² TEMPO-Co-complexes,¹¹³ and tris(4-alkoxyphenyl)amine-Co-complexes,¹¹⁴ were also used in DSSCs to enhance both J_{sc} and V_{oc} simultaneously. A maximum PCE of 11% under 1-sun condition was reported by using tris(4-ethoxyphenyl)amine (TPEA)- $[\text{Co}(\text{bpy})_3]^{3+/2+}$ tandem redox shuttles with an organic dye (see Figure 10).¹¹⁴ The maximum V_{oc} value of around 1.03 V of the device was obtained by using the bulkier tris(butoxyphenyl)-

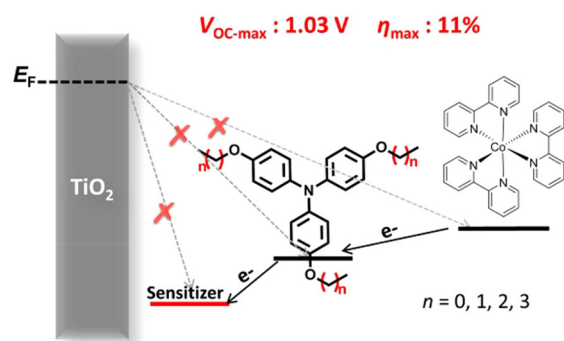


Figure 10. Effect of tris(4-alkoxyphenyl)amine (TPA) mediator on TPA-Co mixed redox shuttles. The recombination of TiO_2 (e^-) was retarded by the steric effect of the TPA mediator. Reprinted with permission from the graphical abstract of ref 114. Copyright 2018 American Chemical Society.

amine (TPBA) in this tris(4-alkoxyphenyl)amine-Co-complex tandem redox shuttle, which was attributed to the suppression of charge recombination by the bulkier butoxy groups in the tris(4-alkoxyphenyl)amine mediator.¹¹⁴ The highest PCE was achieved with the TPEA- $[\text{Co}(\text{bpy})_3]^{3+/2+}$ redox system due to the balanced J_{sc} and V_{oc} values.

4.1.5. Redox Shuttle for Aqueous DSSCs. DSSCs using nitrile-based organic solvents can raise serious concerns about safety in practical applications, especially in indoor photovoltaics due to several drawbacks of organic solvents, such as high vapor pressure, toxicity, and acute environmental impact.¹¹⁵ Regarding the nontoxicity, safe, and eco-friendly nature of water, a 100% aqueous DSSC can be regarded to be a safe and eco-friendly energy source. To date, in most of the cases, the I_3^-/I^- redox shuttle was utilized in aqueous DSSCs.^{116–118} The highest PCE of 7.02% for 100% aqueous DSSCs was achieved under 1-sun illumination by using the I_3^-/I^- redox shuttle with an optimized counter electrode and sensitizer.¹¹⁸ However, there is an increasing issue about iodate formation and stability of the I_3^-/I^- redox shuttle based aqueous DSSCs.¹¹⁹ Organic redox shuttles, such as TEMPO⁺/TEMPO⁰¹²⁰ and thiolate/disulfide (T^-/DS),¹²¹ were also utilized to fabricate aqueous DSSCs, and the PCE under 1-sun condition was in the range of 4–5%. The most important issue about organic redox shuttle based aqueous DSSCs is that the stability of the device was not good.^{120,121} Among metal complexes, the $[\text{Fe}(\text{CN})_6]^{4+/3+}$ redox couple can be a promising candidate due to its noncorrosiveness and similarity of its redox potential to that of I_3^-/I^- . By using the $[\text{Fe}(\text{CN})_6]^{4+/3+}$ redox shuttle and optimizing the device with a carbazole-based dye, Daeneke et al. reported a maximum PCE of 4.2% under 1-sun illumination. However, the photocatalytic degradation of the $[\text{Fe}(\text{CN})_6]^{4+/3+}$ redox couple under white light illumination can cause instability of the device.¹²² Various Co complexes, such as $[\text{Co}(\text{bpy})_3]^{3+/2+}$,^{123,124} $[\text{Co}(\text{phen})_3]^{3+/2+}$,¹²³ were also utilized as redox shuttles for aqueous DSSCs; however, the PCE under 1-sun illumination did not exceed 6% even by optimization of the device in various manners.

4.1.6. Redox Shuttles for p-Type DSSCs. In p-type DSSCs, a dye-sensitized p-type semiconductor film (e.g., NiO) on a TCO substrate works as a photocathode, where the photoexcited dye injects holes into the semiconductor. The reduced dye is then regenerated by the oxidized species of electrolytes. The reduced species of electrolytes inject electrons into the counter electrode. The injected electrons in the counter electrode move to the working electrode through the external circuit and complete the cycle (see Figure 11).

Like n-type DSSCs, the I_3^-/I^- redox couple is mostly used as a redox shuttle in p-type DSSCs. The PCEs of p-type DSSCs are much lower than those of n-type DSSCs due to the large amount of visible light absorbed by typical NiO semiconductors used in p-type DSSCs and small energy gap between I_3^-/I^- (+0.35 V vs NHE) electrolytes and the NiO (+0.70 V vs NHE) semiconductor.^{125–127} Using the $[\text{Co}(\text{en})_3]^{3+/2+}$ ($\text{en} = 1,2$ -diaminoethane) redox shuttle, Powar et al. reported a 1.3% PCE with $V_{\text{oc}} = 0.709$ V under 1-sun condition for p-type DSSCs. The enhanced V_{oc} value was due to the use of the high negative redox potential $[\text{Co}(\text{en})_3]^{3+/2+}$ redox shuttle.¹²⁸ Using the same redox shuttle in an aqueous medium, the same research group further enhanced the maximum PCE to 1.6% under 1-sun condition by controlling $\text{pH} \approx 10$ of the aqueous electrolyte solution.¹²⁹ Perera et al.

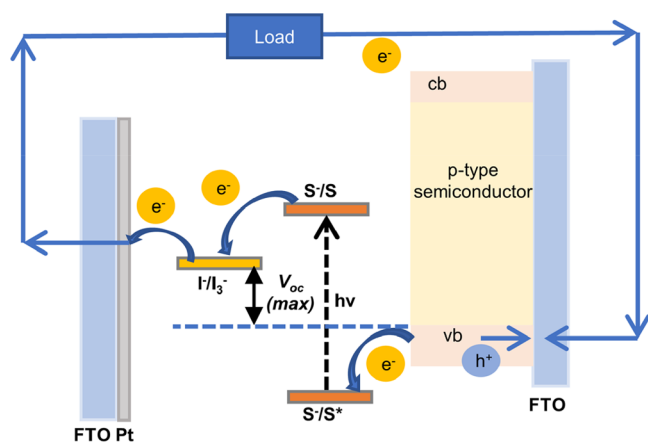


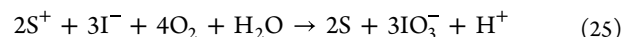
Figure 11. p-Type DSSC device structure with a p-type semiconductor and its working principle.

reported a PCE of up to 2.3% by optimizing a p-type device using an organic-solvent-based $[\text{Fe}(\text{acac})_3]^{0/-}$ (acac = acetylacetonato) redox shuttle with perylene-thiophene-triphenylamine dye (PMI-6T-TPA).¹²⁷ They achieved a maximum J_{sc} of 7.65 mA cm^{-2} by optimizing electrolytes and using a blocking layer on the NiO working electrode.¹²⁷ However, using the more negative redox potential $[\text{Fe}(\text{acac})_3]^{0/-}$ redox shuttle ($E_{\text{redox}} = -0.2 \text{ V vs NHE}$), they did not achieve a high V_{oc} compared to the $[\text{Co}(\text{en})_3]^{3+/2+}$ redox shuttle ($E_{\text{redox}} = -0.03 \text{ V vs NHE}$) device, because of the fast charge recombination across the electrolyte/FTO interface.¹²⁷

4.2. Medium for the Redox Shuttle. The solvent is the medium for the transportation of ionic species in the electrolyte. The choice of the solvent in redox electrolytes depends on the solubility and fast diffusion of the redox shuttle through that medium. Viscosity, boiling point, dielectric constant, and donor number are the important parameters of the solvent when selecting a suitable solvent for the redox electrolytes in DSSCs. Table 1 gives the physical properties of some common solvents for the redox electrolyte system.

The solvent should have low viscosity to enhance the mobility of the carrier ions, a high boiling point to reduce solvent leakage and evaporation problems, high polarity to dissociate the ionic salt, and inertness toward the dye attached on the TiO_2 semiconductor surface or dye–metal oxide bond.

In addition, solvents should have low toxicity and environmental impact. The dielectric constant of the solvent represents a rough estimation of its polarity. The higher the dielectric constant of the solvent, the higher the dissociation capacity of an ionic salt in that medium. The donor number is an empirical parameter to evaluate the nucleophilic property of the solvent. The donor number is defined as the negative ΔH value (kcal mol^{-1}) for the interaction of the electron-pair donor with the standard acceptor SbCl_5 in a diluted 1,2-dichloroethane ($\text{DN} = 0$) medium.¹³⁰ With an increase in the donor number of the solvent, the V_{oc} value significantly increases but J_{sc} decreases.^{131,132} A high donor number (large nucleophilic or basic property) of the solvent causes a negative shift of the TiO_2 conduction band, resulting in the enhancement of the V_{oc} . Due to the negative shift of the TiO_2 conduction band, the driving force for the electron injection from the excited dye to the TiO_2 semiconductor is reduced; as a result, the J_{sc} value decreases because of the reduction in the electron injection efficiency. Therefore, sometimes a mixed solvent can be used to tune the donor number of the medium. For instance, a 90/10 (v/v) mixture of acetonitrile (ACN) and 3-methyl-2-oxazolidinone (NMO) enhances the V_{oc} with minimal loss in J_{sc} , leading to an overall increase in performance.¹³³ From an analysis of efficient DSSCs (see Table 3), it is confirmed that nitrile-based solvents ACN and MPN are the most effective for redox electrolytes; however, they are highly volatile. Fukui et al. also found an 80/20 (v/v) mixture of ACN and tetrahydrofuran (THF) in the I_3^-/I^- electrolyte enhances the V_{oc} with no loss in J_{sc} due to the favorable donating ability of the medium.¹³¹ However, THF is highly volatile and comparatively less polar and can solvate most organic sensitizers. Water was also used as a solvent in DSSCs, due to its safe and eco-friendly nature.^{117,134,135} However, in the I_3^-/I^- redox system, the oxidation of iodide by water and oxygen may produce iodate (IO_3^-) rather than I_3^- (eq 25),¹¹⁹ which causes I_3^- depletion and decreases the device performance.



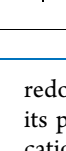

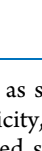




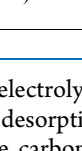
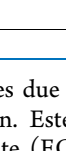

The major limitation of aqueous DSSCs is the low photovoltaic performance due to the mass transport issue¹³⁶ and significant dye desorption, especially with metal-based and hydrophilic dyes.¹³⁷ Alcohols, such as methanol and ethanol,

Table 1. Physical Properties of Some Common Solvents Used for DSSC Redox Liquid Electrolytes^a

solvent	melting point (°C)	boiling point (°C)	viscosity (cP)	dielectric constant	donor number (kcal mol^{-1})
water	0	100	0.89	78.4	18.0
acetonitrile (ACN)	−44	81.6	0.33 (30 °C)	37.5 (20 °C)	14.1
propionitrile (PN)	−93	97	0.39 (30 °C)	27.7	16.1
valeronitrile (VN)	−96.2	141	0.78		
3-methoxypropionitrile (MPN)	−63	164	2.5	36	16.1
tetrahydrofuran (THF)	−108.4	66	0.47 (30 °C)	7.6	20.0
<i>N,N</i> -dimethylformamide (DMF)	−78	133	0.80	36.7	26.6
dimethyl sulfoxide (DMSO)	19	189	2.0	46.5	29.8
sulfolane	27.5	285	10.07		
γ -butyrolactone (GBL)	−44	204	1.7	42	18.0
<i>N</i> -methyl-2-pyrrolidone (NMP)	−24	203	1.65	32.2	27.3
3-methyl-2-oxazolidinone (NMO)	15	266	2.5	77.5	
Ethylene carbonate (EC)	36	238	90	89.1	16.4
Propylene carbonate (PC)	−49	241	2.5	64	15.1

^aAll data at 25 °C and 760 mmHg except where otherwise specified.

Table 2. Structures and Physical Properties of Ionic Liquids Used in DSSC Redox Electrolytes

Ionic liquid	Structure	Melting point (°C)	Viscosity (cP)
1,3-Dimethylimidazolium iodide (DMII)		92	-
1-Ethyl-3-methylimidazolium iodide (EMII)		77.5	-
1-Methyl-3-propylimidazolium iodide (PMII)		17	865
1-Butyl-3-methylimidazolium iodide (BMII)		-72	963
1-Hexyl-3-methylimidazolium iodide (HMII)		-75	1439
1,2-Dimethyl-3-propylimidazolium iodide (DMPII)		94	-
1,2-Dimethyl-3-hexylimidazolium iodide (DMHII)		< 100	-
1-Ethyl-3-methylimidazolium tetracyanoborate (EMIB(CN) ₄)		13	19.8 (20 °C)
1-Ethyl-3-methylimidazolium tricyanomethanide (EMITCM)		-10	18 (20 °C)
1-Butyl-3-methyltriazolium iodide (BMTI)		< 100	-

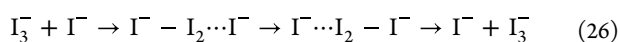
are not suitable as solvents in DSSC redox electrolytes due to their hydrophilicity, which can cause dye desorption. Ester- and lactone-based solvents, such as ethylene carbonate (EC), propylene carbonate (PC), and γ -butyrolactone (GBL), are also used in DSSCs due to their lower volatility and high dielectric constant.^{66,132,138} EC has a high melting point (~ 36 °C) and high viscosity. Therefore, a cosolvent is required with EC. However, the performance of these solvents cannot overcome the performance of the ACN-based solvent due to the mass transport limitation of the redox shuttle in these media. GBL has potential as a solvent for DSSC redox electrolytes compared to other lactone-based solvents due to its low melting point (~ -44 °C), high boiling point (~ 204 °C), moderate donor number (18), and comparatively low viscosity (~ 1.7 cP). *N*-Methyl-2-pyrrolidone (NMP) has a high donor number (high basicity), so it can simultaneously enhance the V_{oc} and decrease the J_{sc} value.

4.3. Ionic Liquids. An ionic liquid (IL) is a salt whose melting point is below 100 °C or even at room temperature. The IL is composed of at least one organic ion (usually a cation) with a delocalized charge to prevent a stable crystal lattice. Due to the loosely coordinating bonds between ions, the melting point is below 100 °C. An IL can be an alternative to volatile organic solvents due to several advantages, such as negligible vapor pressure even at the high temperature of the solar cell operation, high electrochemical stability, wide electrochemical window, and the ability to dissociate a wide range of organic and inorganic compounds. Generally, the viscosity of an IL is around 10–500 cP.¹³⁹ Thus, ILs are far more viscous than the common organic solvents used in DSSC

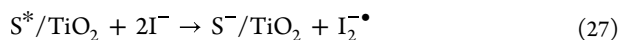
redox electrolytes. The IL is called a “tunable” solvent because its physicochemical properties can be varied by modifying the cationic or anionic components.¹⁴⁰ The high viscosity of ILs causes a mass transport limitation of the redox shuttle. A relatively low viscosity and hydrophobicity of ILs are essential for their use in redox electrolytes for DSSCs. Table 2 shows the structure and physical properties of the most common ILs used in DSSC redox electrolytes.

In the 1-alkyl-3-methylimidazolium iodide series, compounds with an alkyl chain from propyl (C3) to nonyl (C9) are viscous liquids, and their viscosity increases with increasing alkyl chain length due to the increasing van der Waals interactions. Kubo et al. studied a series of 1-alkyl-3-methylimidazolium iodide ionic liquids with alkyl chain lengths from C3 to C9 as molten salts in iodine electrolytes and found that the 1-hexyl-3-methylimidazolium iodide molten salt electrolyte had the best photovoltaic performance despite having a higher viscosity and conductivity than the lower alkyl chain length members.¹⁴¹ The J_{sc} value increases with increasing alkyl chain length from propyl (C3) to heptyl (C7) and then decreases for longer chain lengths. They reported that the reason for the J_{sc} value increasing with increasing alkyl chain length from C3 to C7 is due to the enhanced diffusion coefficient of electrons in the TiO₂/electrolyte system. The increasing alkyl chain length increases the van der Waals interaction and aggregation of the 1-alkyl-3-methylimidazolium cation, which could enhance the adsorption of this cation onto the TiO₂ surfaces. As a consequence, the J_{sc} value may increase with increasing diffusion of electrons in TiO₂ due to the enhanced adsorption of the 1-alkyl-3-

methylimidazolium cation.^{141,142} In the imidazolium-based ionic liquid, the viscosity can be reduced by changing its counteranion to a loosely coordinating anion.¹³⁹ 1-Ethyl-3-methylimidazolium iodide (EMII) is solid at room temperature, and the viscosity of the 1-ethyl-3-methylimidazolium (EMI) cation based ionic liquid decreased in the following order: $\text{EMI}^+(\text{PF}_6)^- < \text{EMI}^+(\text{BF}_4)^- < \text{EMI}^+[\text{N}(\text{CF}_3\text{SO}_2)_2]^- < \text{EMI}^+(\text{CF}_3\text{COO})^- < \text{EMI}^+[\text{B}(\text{CN})_4]^-$ or $\text{EMI}^+[\text{C}(\text{CN})_3]^-$.^{143–145} Wang et al. achieved a remarkable efficiency of 7.4% under 1-sun illumination completely using ionic liquids as the solvent.¹⁴³ They used binary ionic liquids, 1-propyl-3-methylimidazolium iodide (PMII) and 1-ethyl-3-methylimidazolium tricyanomethanide (EMITCM), as nonvolatile solvents. The viscosities of EMITCM and PMII are around 18 cP (at 22 °C) and 865 cP (at 25 °C), respectively.^{141,146} Thus, due to the loosely coordinating bond between the tricyanomethanide (TCM) anion and the 1-ethyl-3-methylimidazolium (EMI) cation, the viscosity of the EMITCM ionic liquid is significantly reduced. The reason for using binary ionic liquids is to reduce the viscosity of the media; therefore, the mass transport limitation of the redox shuttle can be suppressed. Kuang et al. reported a 7.6% efficiency at simulated 1 sun illumination using 65% PMII with 35% 1-ethyl-3-methylimidazolium tetracyanoborate ($\text{EMIB}(\text{CN})_4$) as binary ionic liquids in organic-solvent-free I_3^-/I^- redox electrolytes. They also claimed this binary ionic liquid based device was highly stable even at 80 °C in the dark. During a 1000 h accelerated test under 80 °C and dark conditions, they claimed that their device was able to retain more than 90% of its initial efficiency.¹⁴⁷ Due to the high viscosity of the ionic liquid, when the ionic liquid is used as a solvent in redox electrolytes, a high concentration of the redox shuttle is required to compensate for the mass transport limitation for fast dye regeneration. The Grotthus-type charge transport mechanism (eq 26) may affect the overall transport with increasing iodide concentration in ionic-liquid-based I_3^-/I^- redox electrolytes.⁶³



Thus, triiodide might transfer to the counter electrode not only by diffusion but also by other nondiffusional hopping type mechanisms.^{63,148} However, a high concentration of the redox shuttle (iodide species) can increase the probability of the reductive quenching of the excited dye.¹⁴⁹ Wang et al. discovered evidence of the reductive quenching of the dye excited state by a very high iodide concentration (eq 27) in PMII ionic-liquid-based I_3^-/I^- redox electrolytes. They also reported from their transient laser experiment that reduced dye species (S^-) do not inject electrons into the TiO_2 conduction band; rather, they decay by a slow reaction process ($t_{1/2} \approx 1$ ms) with oxidized species of electrolytes (I_3^-).¹⁴³



Thus, reductive quenching of the excited dye can cause a low photocurrent of the device. The short-circuit current density and PCE of the device decrease with increasing viscosity of the ionic liquid.¹⁴⁸ From a comparison of the impedance of the room-temperature ionic liquid (RTIL) and liquid solvent based cells, it was determined that a higher recombination and lower injection efficiency are the main causes of the limiting performance of RTIL-based cells.¹⁴⁷ Due to the limitation of the performance, the ionic liquid is not suitable as a single solvent in redox electrolytes; rather, it can be mixed with an organic solvent to enhance the performance

of the device. Despite the high viscosity and mass transport limitation of the RTILs, several attempts have been made to use an RTIL as a single nonvolatile solvent in DSSCs to enhance both the performance and stability of the devices. Shi et al. tested two types of redox liquid electrolytes: a low-volatility electrolyte (1) organic solvent MPN with a combination of an ionic liquid salt DMII and additives in the I_3^-/I^- redox couple and a nonvolatile electrolyte (2) fully organic-solvent-free mixed ionic liquids EMII, $\text{EMIB}(\text{CN})_4$ with a combination of DMII and the same additives.¹⁵⁰ They obtained an efficiency of 9.6% for the organic solvent based low-volatility electrolytes and 8.6% for the fully ionic liquid based nonvolatile electrolytes under standard AM 1.5G illumination. However, in a long-term stability test, both low-volatility organic solvent based and nonvolatile ionic liquid based devices were stable with an insignificant difference (efficiency dropping 9% for the low-volatility electrolytes and 6% for the ionic liquid electrolytes) under 60 °C and full sunlight for 1000 h.¹⁵⁰ Recently, Bousrez et al. reported that the 1-alkyl-3-methyltriazolium iodide ionic liquids can be more suitable in DSSC electrolytes over imidazolium iodides due to their less hygroscopic nature. In the 1-alkyl-3-methyltriazolium iodide series, compounds with an alkyl chain length from C4 to C10 exhibit the characteristics of ionic liquids. They found that the 1-butyl-3-methyltriazolium iodide ionic liquid based device showed the best efficiency of 6.63% under 40 °C and 1-sun conditions.¹⁵¹

Although ionic liquids limit mass transport due to their high viscosity, this class of compounds has great potential due to the enhancement of the stability of the device. Under ambient light conditions, the operation of the device requires a lower mass transport of the redox shuttle due to the lower photocurrent generated by the dye in low light. Therefore, in indoor photovoltaics, the ionic liquid can play a significant role as a nonvolatile solvent. By proper optimization of the device, the PCE under 1 sun may also be enhanced to a certain extent. The most important use of this class of compounds can be as additives in organic solvent based liquid redox electrolytes and iodide sources of I^-/I_3^- redox electrolytes.

4.4. Additives for the Redox Electrolytes. Additives are certain compounds whose presence in electrolytes can improve the photovoltaic performance of the solar cell. The common additives used in DSSC redox electrolytes are shown in Scheme 2.

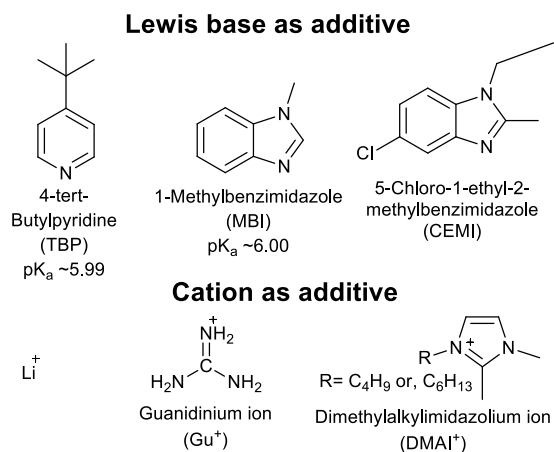
Nazeeruddin et al. first reported that a TBP treatment in a dye-sensitized TiO_2 electrode significantly enhanced the V_{oc} and fill factor of the device due to the suppression of the interfacial recombination reaction between the injected electrons in TiO_2 and the oxidized species of the redox couple.¹³³ The V_{oc} value for DSSCs with the I_3^-/I^- redox electrolyte can be expressed by eq 28¹³³

$$V_{oc} = \frac{kT}{q} \ln \left(\frac{I_{inj}}{n_{cb} k_{rec} [\text{I}_3^-]} \right) \quad (28)$$

where I_{inj} is the flux of the charge from injection by the sensitizer to the TiO_2 semiconductor, n_{cb} is the carrier electron density on the conduction band of TiO_2 , and k_{rec} is the rate constant of the interfacial recombination reaction (back electron transfer from TiO_2 to I_3^- ; see eq 29).



Scheme 2. Structures of the Most Effective Additives in DSSC Redox Electrolytes



Therefore, the V_{oc} value can be enhanced by reducing the rate of the interfacial recombination reaction (eq 28). Adsorption of electron-donating TBP at the electron-accepting TiO_2 sites causes passivation at the TiO_2 surface, which suppresses the back electron transfer from TiO_2 to the oxidized species (electron acceptor) of the electrolytes and reduction in the electron injection efficiency from the excited dye. Boschloo et al. quantified the effect of the addition of TBP to the I_3^-/I^- redox electrolytes in DSSCs. From the charge extraction and electron lifetime measurement, they concluded that the increase in the V_{oc} of around 260 mV due to the addition of 0.5 M TBP in MPN solvent based I_3^-/I^- electrolytes could be attributed to both a shift of the TiO_2 conduction band toward negative potential ($\sim 60\%$ contribution) and an enhancement of the electron lifetime ($\sim 40\%$ contribution).¹⁵² The adsorption of TBP on the TiO_2 surface may decrease the chance of I_3^- accessing the TiO_2 surface. The increase in the electron lifetime may be attributed to the blocking effect of TBP and the complexation of free iodine with TBP, which is much more pronounced at higher TBP concentrations and for the MPN-based solvent than for the acetonitrile solvent.¹⁵² However, the major factors for V_{oc} enhancement can be attributed to the shifting of the TiO_2 conduction band edge toward negative potential^{153,154} to suppress the interfacial recombination reaction of the injected electron and oxidized species (electron acceptor) of the redox electrolytes.^{133,155} Besides, the presence of TBP may decrease the amount of adsorbed protons and cations on the TiO_2 surface. However, TBP and pyridine can be adsorbed readily on the Pt surface by its nitrogen atom in the aromatic ring.^{156,157} Kim et al. studied the effect of TBP on DSSC electrodes. They found from the EIS measurement of the Pt-FTO/iodine electrolytes/Pt-FTO cell that the catalytic effect of Pt can deteriorate and the diffusion resistance of electrolytes can be increased by a higher TBP concentration (>0.5 M).¹⁵⁸ There is no measurable influence on the charge transfer resistance in the counter electrode and the diffusion due to the addition of TBP in Co^{3+}/Co^{2+} complex redox electrolytes. However, TBP harms the charge transfer in the counter electrode and the diffusion in the Cu^{2+}/Cu^+ complex redox system.¹⁰⁶ The Cu(II) species is the diffusion-controlling ion (low concentration of Cu(II) species) in the Cu(II)/Cu(I) redox system. The Cu(II) species is susceptible to altering its coordination sphere, which may influence its coordination geometry and increase its coordina-

tion number from 4 to 6. The substitution of the ligand by TBP, solvent, and/or counterions in the Cu(II) complex may happen.¹⁵⁹ The Cu(II) species in the redox solution can become bulky and hydrophobic due to this change.¹⁰⁶ Therefore, the reduced charge transfer and diffusion can be observed due to the changes of the Cu(II) species. Ferdowsi et al. found correlations of the basicity (pK_a) of the pyridine bases with the charge transfer rate in the PEDOT counter electrode and the diffusion resistances of the copper redox mediator. By studying the series of pyridine bases, they found that an increase in the basicity of the pyridine bases leads to a decrease in the formal rate constant of the charge transfer and an increase in the diffusion coefficient.¹⁶⁰ However, a weak Lewis base like 2,6-bis-*tert*-butylpyridine ($pK_a \approx 3-4$) is ineffective in increasing V_{oc} by shifting the TiO_2 conduction band edge upward. Therefore, bases with a pK_a value near 6.0 like TBP and 4-(5-nonyl)pyridine can be effective in enhancing the V_{oc} and the overall performance of the solar cell.

The pK_a value of 1-methylbenzimidazole or *N*-methylbenzimidazole (MBI or NMB) (~ 6.0)¹⁶¹ is almost the same as that of TBP. The role of MBI as an additive in DSSC redox electrolytes is also the same as that of TBP: i.e., an improvement in the V_{oc} value by shifting the TiO_2 conduction band edge to a more negative potential and enhancing the electron lifetime on the TiO_2 surface.¹⁶² Like TBP, MBI may also affect the TiO_2 surface charge by reducing the Li^+ ion adsorption on the TiO_2 surface and may suppress the back electron transfer to the electron acceptor species of electrolytes by interacting with them.¹⁶³ Recently, it was found that the effect of MBI in enhancing V_{oc} is much more pronounced than that of TBP in I_3^-/I^- electrolytes.¹⁹ However, MBI reduces the J_{sc} value more in comparison with TBP probably due to the lower electron injection efficiency by a higher upshift of the TiO_2 conduction band. There was no significant difference in the overall PCE and stability of the device due to the use of either the TBP or MBI additive in I_3^-/I^- electrolytes.¹⁹ The best power conversion efficiencies for copper complex redox mediators have been achieved by using the MBI additive (see Table 3). Therefore, MBI may be more suitable as a Lewis base additive in copper electrolytes over TBP. Recently, Furer et al. studied the role of Lewis base additives in the copper redox mediator.¹⁶⁴ They concluded from their CV analysis that the coordination of strong Lewis bases like TBP and MBI with the Cu(II) complex (coordination number 4) is the main factor for efficient blocking of the electron recombination with the Cu(II) species (see Figure 12).

Furer et al. achieved the best efficiency with the MBI additive in $[Cu(dmp)_2]^{2+/+}$ redox mediators mainly due to the improvement in V_{oc} with minimal sacrifice of the J_{sc} value.¹⁶⁴ However, it is still unclear why the J_{sc} value is more reduced in the case of TBP rather than the MBI additive in $Cu(dmp)^{2+/+}$ redox electrolytes. They also claimed that a weak Lewis base additive, which may not coordinate with the Cu(II) center, can reduce the photovoltaic performance due to a higher charge recombination. The possibly rational reasons for the low cell performance with weak LB additive are the inability of a weak LB additive to increase V_{oc} by shifting the TiO_2 conduction band edge upward¹⁶⁰ and the ineffectiveness in blocking charge recombination processes. The binding or coordination of Cu(II) complexes with the additional Lewis base additive TBP or MBI may slow down the reduction of the Cu(II) species at the counter electrode¹⁶⁴ and complicate the redox process. It should be noted that the binding or coordination of

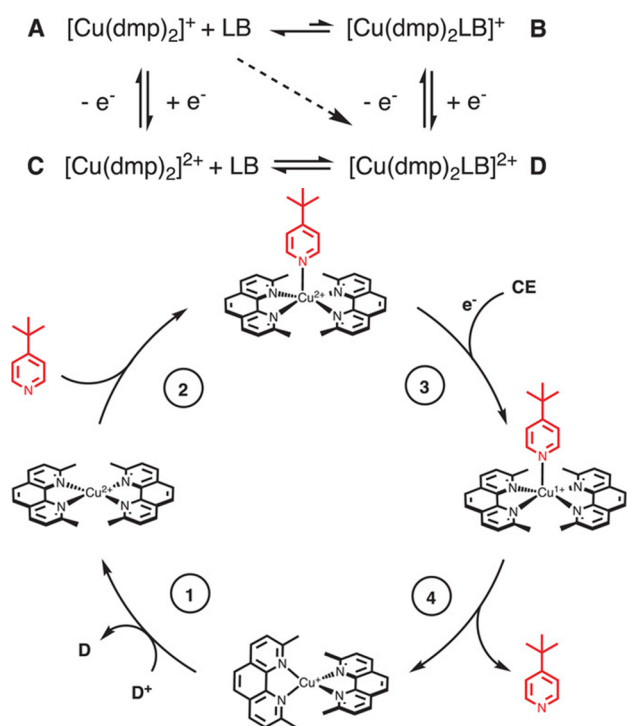


Figure 12. Effect of the coordination of an additional Lewis base (LB) on the oxidation and reduction in copper complexes, with the most favorable paths for oxidation and reduction being ACD and DBA, respectively, and the possible mechanism of dye regeneration and electrolyte regeneration by copper complexes in the presence of LB. Reprinted with permission from ref 164. Copyright 2020 Wiley.

Cu(II) complexes can negatively shift the redox potential,^{165,166} which can enhance the rate of the charge recombination reaction due to the lower driving force for recombination.¹⁶⁶ Recently, Ren et al. obtained a high FF without sacrificing J_{sc} and V_{oc} by using a 5-chloro-1-ethyl-2-methylimidazole (CEMI) additive in $[\text{Cu}(\text{tmby})_2]^{2+/+}$ redox electrolytes instead of using MBI.²⁹ The high FF may be due to the low interfacial transport resistance between the electrolyte and the counter electrode. The comparable J_{sc} and V_{oc} values with MBI additive indicate a similar interaction of $[\text{Cu}(\text{tmby})_2]^{2+/+}$ and CEMI.

The adoption of certain cations also affects the performance of the DSSC. From laser-pulse-induced photocurrent transient measurements, Kambe et al. found that the photogenerated electron in the TiO_2 electrode increases in the order $\text{DMHI}^+ < \text{TBA}^+ < \text{Na}^+ < \text{Li}^+$.¹⁴² At high concentrations, the adsorption of Li^+ on the TiO_2 surface boosts the photogeneration of electrons and also increases the electron diffusion coefficient in the TiO_2 electrode. The multilayer adsorption of the imidazolium cation, DHMI^+ , increases electron diffusion to a great extent but lowers the photogeneration of electrons.¹⁴² The presence of a high concentration of both Li^+ and imidazolium cations in the electrolyte solution may be beneficial due to the increase of electron diffusion and the optimum photogeneration of electrons. Guanidinium thiocyanate (GuSCN) is also used as an additive in DSSC redox electrolytes. The guanidinium cation affects the photocurrent in the same way as other cations, shifting the TiO_2 conduction band toward a positive potential, which increases the electron injection efficiency.¹⁶⁷ The adsorbent Gu^+ suppresses the electron recombination at the TiO_2 /electrolyte surface by

passivating recombination sites. The net effect of the downward shift of the TiO_2 conduction and slower recombination due to the adsorbent Gu^+ may increase the overall V_{oc} up to 20 mV.¹⁶⁸ Like Li^+ , intercalation of Gu^+ into TiO_2 is not anticipated. However, Kopidakis et al. reported that the Li^+ interaction in the TiO_2 film does not affect the photovoltaic performance of the DSSC and only has a small influence on the charge collection efficiency and the rate of recombination.¹⁶⁹

5. PROGRESS OF PHOTOVOLTAIC PERFORMANCE OF DSSCs BY LIQUID REDOX ELECTROLYTES

5.1. Under 1-Sun Illumination. In Table 3, the outstanding photovoltaic performances of DSSCs by using redox liquid electrolytes under standard AM 1.5G (100 mW cm^{-2}) illumination are summarized. The significant PCEs of 11.7% and 12.4% with a ruthenium dye⁶⁸ and concerted companion dye,¹⁰ respectively, for I_3^-/I^- redox shuttles, 14.3% with two cosensitized organic dyes, for a $\text{Co}^{3+}/\text{Co}^{2+}$ redox shuttle, and 15.2% with two cosensitized organic dyes⁸ for a $\text{Cu}^{2+}/\text{Cu}^+$ redox shuttle have been reported under standard AM 1.5G (1-sun) illumination by optimizing the dye structure, the counter electrode, and device fabrication.

5.2. Under Ambient Light Conditions. The intensity of indoor light is much lower than that of outdoor light. The spectra of ambient light also vary significantly with the solar emission spectra. In Figure 13, a comparison of the emission spectra of fluorescence and LED bulbs with the spectra of AM 1.5G standard is shown.¹⁷³ The intensity of standard indoor light is around 200–2000 lx, which is around 0.2–2% of the full sun (100 mW cm^{-2} , AM 1.5G) illumination (100000 – 110000 lx).

The low photocurrent is generated by indoor light conditions. Therefore, a low concentration of the redox couple is required to operate the solar cell and for efficient dye regeneration. The reduced concentration of redox species in electrolytes for indoor light conditions suppresses the interfacial charge recombination.⁸ Outstanding performances under ambient light have already been achieved for DSSCs. The exciting performances for liquid-state DSSCs under ambient light conditions reported in the literature are shown in Table 4. A record power conversion efficiency of 34.5% was reported for DSSCs by using copper complex redox shuttles.⁸ The outstanding performances of DSSCs under indoor light conditions make this technology a promising and clean energy source to integrate in IoT and low-energy-consumption electronic devices.

6. SUMMARY AND OUTLOOK

The redox electrolyte is the major component of a DSSC, which affects the PCE and long-term stability of the device. By using an I_3^-/I^- redox shuttle, a remarkable PCE of up to 12.4% has been achieved under 1-sun illumination. However, its low positive redox potential restricts the V_{oc} of the device to 0.8 V. Also, its drawbacks, such as competitive visible light absorption with dye, corrosiveness toward metal, and volatile nature of iodine, limit the large-scale module development by using the I_3^-/I^- redox shuttle. Thus, Co complex based redox shuttles with a high V_{oc} value have received great attention due to the less competitive visible light absorption, with tuning of the redox potential by replacing ligands. An outstanding PCE of over 14% has been achieved by using the $[\text{Co}(\text{bpy})_3]^{3+/+}$

Table 3. Progress of the Photovoltaic Performances of DSSCs Using Various Redox Electrolytes under Simulated 1-Sun (Standard AM 1.5G, 100 mW cm⁻²) Conditions

redox shuttle (electrolyte composition)	sensitizer (type)	counter electrode catalyst	reported efficiency (V _{oc} /J _{sc} FF)	year, ref
I ₃ ⁻ /I ⁻ (1.0 M DMII, 50 mM LiI, 30 mM TBP, 0.1 M GNCS in the mixture of ACN and VN (85/15))	C106 (Ru complex) + CDCA (coadsorbent)	Pt	11.7% (0.758 V, 19.78 mA cm ⁻² , 0.779)	2010, Yu et al. ⁶⁸
I ₃ ⁻ /I ⁻ (0.6 M DMPH, 0.05 M I ₂ , 0.1 M LiI and 0.4 M TBP in ACN)	Black dye (Ru complex) + Y1 (coadsorbent)	Pt	11.4% (0.743 V, 21.3 mA cm ⁻² , 0.770)	2012, Han et al. ⁶⁹
I ₃ ⁻ /I ⁻ (0.1 M LiI, 0.05 M I ₂ , 0.6 M PMII and 0.5 M TBP in ACN)	XW61 (D-π-A structure, organic and porphyrin dye linked with nonconjugated bridging group) + CDCA (coadsorbent)	Pt	12.4% (0.775 V, 21.41 mA cm ⁻² , 0.747)	2020, Zeng et al. ¹⁰
Co ³⁺ /Co ²⁺ (0.22 M [Co ²⁺ (bpy) ₃](BCN) ₄), 0.05 M [Co ³⁺ (bpy) ₃](BCN) ₄), 0.1 M LiClO ₄ , and 0.8 M TBP in ACN)	SGT-021 (porphyrin, D-π-A structure) + HC-A4 (coadsorbent)	Pt	12.1% (0.910 V, 17.50 mA cm ⁻² , 0.753)	2016, Kang et al. ⁴
Co ³⁺ /Co ²⁺ (0.25 M [Co ²⁺ (bpy) ₃](TFSI) ₂ , 0.06 M [Co ³⁺ (bpy) ₃](TFSI) ₃ , 0.1 M LiTFSI, and 0.5 M TBP in ACN)	SGT-021 (porphyrin, D-π-A structure) + HC-A1 (coadsorbent)	Pt	12.6% (0.849 V, 19.2 mA cm ⁻² , 0.768)	2019, Zhou et al. ⁷⁷
Co ³⁺ /Co ²⁺ (0.25 M [Co ²⁺ (bpy) ₃](TFSI) ₂ , 0.06 M [Co ³⁺ (bpy) ₃](TFSI) ₃ , 0.1 M LiTFSI, and 0.5 M TBP in ACN)	SM315 (porphyrin, D-π-A structure) + CDCA (coadsorbent)	graphene nanoplatelet (GNP)	13.0% (0.91 V, 18.1 mA cm ⁻² , 0.78)	2014, Mathew et al. ¹⁰⁵
Co ³⁺ /Co ²⁺ (0.22 M [Co ²⁺ (bpy) ₃](B(CN) ₄) ₂ , 0.05 M [Co ³⁺ (bpy) ₃](B(CN) ₄) ₃ , 0.1 M LiClO ₄ , and 0.8 M TBP in ACN)	SM315 (porphyrin, D-π-A structure) + CDCA (coadsorbent)	N and S codoped mesoporous carbons	12.72% (0.893 V, 18.78 mA cm ⁻² , 0.759)	2017, Kim et al. ¹⁷⁰
Co ³⁺ /Co ²⁺ (0.22 M [Co ²⁺ (bpy) ₃](B(CN) ₄) ₂ , 0.05 M [Co ³⁺ (bpy) ₃](B(CN) ₄) ₃ , 0.1 M LiClO ₄ , and 0.85 M TBP in ACN)	ZL003 (organic, D-π-A structure) + CDCA (coadsorbent)	Pt	12.23% (0.873 V, 19.17 mA cm ⁻² , 0.731)	2019, Zhang et al. ⁷¹
Co ³⁺ /Co ²⁺ (0.20 M [Co ²⁺ (phen) ₃](PF ₆ ⁻) ₂ , 0.05 M [Co ³⁺ (phen) ₃](PF ₆ ⁻) ₃ , 0.07 M LiClO ₄ , 0.02 M NaClO ₄ , 0.03 M TBAPF, 0.01 M TBPPF, 0.01 M HMIMPF, 0.30 M TBP, 0.10 M TMSP, 0.10 M MP, 0.05 M CP4BP, 0.10 M CPeBP, and 0.05 M COeBP in ACN)	ADEKA-1 + LEG4 (organic D-π-A structure)	Au/graphene nanoplatelet	14.3% (1.013 V, 18.36 mA cm ⁻² , 0.754)	2015, Kakiage et al. ¹¹
Co ³⁺ /Co ²⁺ (0.22 M [Co ²⁺ (bpy) ₃](B(CN) ₄) ₂ , 0.05 M [Co ³⁺ (bpy) ₃](B(CN) ₄) ₃ , 0.1 M LiClO ₄ , and 0.8 M TBP in ACN)	SGT-137 (organic D-π-A structure) + HC-A1 (coadsorbent)	Pt	12.45% (0.884 V, 18.37 mA cm ⁻² , 0.767)	2017, Yom et al. ⁵
Co ³⁺ /Co ²⁺ (0.25 M [Co ²⁺ (bpy) ₃](TFSI) ₂ , 0.10 M [Co ³⁺ (bpy) ₃](TFSI) ₃ , 0.1 M TBP, and 0.1 M LiTFSI in ACN)	SGT-137 (organic D-π-A structure) + HC-A1 (coadsorbent)/SGT-021 (porphyrin D-π-A structure) + HC-A4 (coadsorbent)	parallel tandem cell	14.64% (0.878 V, 22.06 mA cm ⁻² , 0.756)	
Co ³⁺ /Co ²⁺ (0.22 M [Co ²⁺ (bpy) ₃](TFSI) ₂ , 0.05 M [Co ³⁺ (bpy) ₃](TFSI) ₃ , 0.1 M LiTFSI, and 0.8 M TBP in ACN)	Blue dye, R6 (organic D-π-A structure)	Pt	12.6% (0.850 V, 19.69 mA cm ⁻² , 0.754)	2018, Ren et al. ⁸⁰
Co ³⁺ /Co ²⁺ (0.22 M [Co ²⁺ (bpy) ₃](TFSI) ₂ , 0.05 M [Co ³⁺ (bpy) ₃](TFSI) ₃ , 0.1 M LiTFSI, and 0.8 M TBP in ACN)	SGT-149 (organic D-π-A structure) + SGT-021 (porphyrin D-π-A structure) + HC-A1 (coadsorbent)	Pt	14.2% (0.919 V, 21.06 mA cm ⁻² , 0.734)	2020, Ji et al. ⁹
Co ³⁺ /Co ²⁺ (0.22 M [Co ²⁺ (bpy) ₃](PF ₆ ⁻) ₂ , 0.05 M [Co ³⁺ (bpy) ₃](PF ₆ ⁻) ₃ , 0.1 M LiClO ₄ , 0.2 M TBP, and 0.1 M TPEA in ACN)	AQ310 (organic D-A-π-A structure)	PEDOT	11.0% (0.950 V, 15.5 mA cm ⁻² , 0.745)	2018, Hao et al. ¹¹⁴
Cu ²⁺ /Cu ⁺ (0.09 M [Cu ²⁺ (tmby) ₂](TFSI) ₂ , 0.20 M [Cu ⁺ (tmby) ₂](TFSI), 0.1 M LiTFSI, and 0.6 M NMB in ACN)	Y123 + XY1b (organic D-π-A structure) + CDCA (coadsorbent)	PEDOT	13.1% (1.05 V, 15.74 mA cm ⁻² , 0.79)	2018, Cao et al. ¹²
Cu ²⁺ /Cu ⁺ (0.2 M [Cu ²⁺ (tmby) ₂](TFSI), 0.09 M [Cu ⁺ (tmby) ₂](TFSI) ₂ , 0.1 M LiTFSI, and 0.6 M NMB in ACN)	R7 + Y123 (organic D-π-A structure)	PEDOT	12.7% (1.04 V, 16.15 mA cm ⁻² , 0.761)	2020, Ren et al. ¹⁷²
Cu ²⁺ /Cu ⁺ (0.2 M [Cu ²⁺ (tmby) ₂](TFSI), 0.1 M [Cu ⁺ (tmby) ₂](TFSI) ₂ , 0.1 M LiTFSI, and 0.6 M NMB in ACN)	MSS + XY1b (organic, D-π-A structure) + CDCA (coadsorbent)	PEDOT	13.5% (1.05 V, 15.84 mA cm ⁻² , 0.813)	2021, Zhang et al. ⁸
Cu ²⁺ /Cu ⁺ (0.16 M [Cu ²⁺ (tmby) ₂](TFSI), 0.08 M [Cu ⁺ (tmby) ₂](TFSI) ₂ , 0.1 M NaTFSI, and 0.45 M CEMI in ACN)	SL9 + SL10 (organic, D-π-A structure) + BPHA (preadsorbent)	PEDOT	15.2% (1.04 V, 17.8 mA cm ⁻² , 0.821)	2022, Ren et al. ²⁹

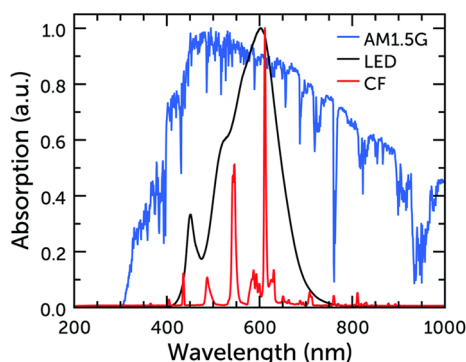


Figure 13. Normalized emission spectra of different ambient light bulbs and AM 1.5G standard. Reprinted with permission from ref 172. Copyright 2021 Royal Society of Chemistry.

[Co(bpy)₃]²⁺ redox shuttle, however, slow mass transport and large reorganization energy in the counter electrode still limit the V_{oc} value to 1 V. Recently, using a Cu complex, a [Cu(tmby)₂]²⁺/[Cu(tmby)₂]⁺ redox shuttle, the PCE of DSSC under 1-sun illumination has reported to be 15.2% with a V_{oc} of over 1 V. Although the V_{oc} value was improved significantly by using the [Cu(tmby)₂]²⁺/[Cu(tmby)₂]⁺ redox shuttle, further improvement of J_{sc} value using this redox shuttle is difficult, due to the competition of the visible light absorption of Cu complexes and the requirement of using a dye with a higher positive HOMO level, which limits the scope of the entire range of visible light utilization. Due to the higher positive redox potential of [Cu(tmby)₂]²⁺/[Cu(tmby)₂]⁺ complexes (~ 0.87 V vs NHE), most of the developed high-efficiency porphyrin dyes, such as SM315 ($E_{HOMO} \approx 0.89$ V),¹⁰⁵ SGT-021 ($E_{HOMO} \approx 0.82$ V),⁴ and XW17 ($E_{HOMO} \approx 0.68$ V),¹⁷⁸ some organic dyes, such as SGT-149 ($E_{HOMO} \approx 0.84$),⁹ and near-infrared (NIR) absorbing organic dyes, such as ISQ1 ($E_{HOMO} \approx 0.62$ V)¹⁷⁹ and AP3 ($E_{HOMO} \approx 0.74$ V),¹⁷⁸ cannot be explored with this Cu redox shuttle because of the insufficient driving force for dye regeneration. Therefore, research is needed to find a suitable redox shuttle with a redox potential of 0.45–0.65 V or replacement of a ligand to tune the redox potential of the Cu complexes, so that most of the porphyrin and organic dyes can be utilized.

It has been assessed that the commercial application of DSSCs for outdoor applications may be possible and economically beneficial if the PCE of the device exceeds 15% under 1-sun illumination³⁰ and the device retains high stability under light-soaking at a high temperature (~ 60 °C).¹⁸⁰ Therefore, as proposed and depicted in Scheme 3 for the PCE enhancement of over 16% (1) simultaneously improving J_{sc} to over 21 mA/cm² and V_{oc} to 1.0 V of the device can be feasible by utilizing cosensitization of currently developed organic/porphyrin dyes with a NIR-absorbing dye and redox shuttles with a redox potential around 0.45–0.65 V and (2) improving the FF to 0.80 can be possible by using a superior counter electrode catalyst with a specific redox shuttle and proper device optimization.^{29,170,181,182}

Redox shuttles with a redox potential around 0.45–0.65 V can give a theoretical V_{oc} in the range of 0.95–1.15 V. The use of cosensitization of previously developed porphyrin, organic, and NIR absorbing dyes can broaden whole visible light absorption, which surely can enhance the J_{sc} value by entire visible light utilization. Depending on the cosensitization system and maintenance of an optimum driving force of ~ 0.2 –

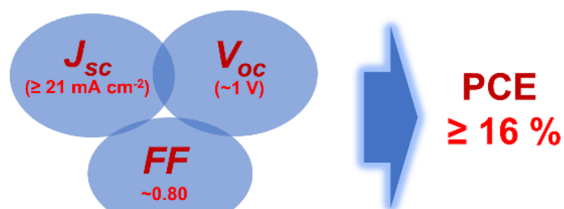
Table 4. Progress of the Photovoltaic Performances for DSSCs Using Various Redox Electrolytes under Ambient Light Illumination

liquid electrolyte composition	sensitizer	counter electrode catalyst	light source	illumination	reported efficiency (V_{oc} FF)	year, ref.
I ₃ ⁻ /I ⁻ (0.07 M LiI, 1 M PMII, 0.05 M I ₂ , 0.05 M TBP in ACN/VN (85:15, v/v))	anthracene-based D-A- π -A sensitizer (TY6) + CDCA (coadsorbent)	PVP-Pt	T5-fluorescent lamp	1200 lx, $P_{in} = 345$ μ W cm ⁻²	24.4% (0.671 V, 164 μ A cm ⁻² , 0.778)	2017, Tingare et al. ¹⁷⁴
I ₃ ⁻ /I ⁻ (EL-HPE; iodine, inorganic iodide salt, pyridine derivatives in ACN and VN solvent mixture)	N719 + CDCA (coadsorbent)	Pt	LED (Osram, class A, 86 W, 2700 K)	$P_{in} = 1577$ μ W cm ⁻²	28.7% (0.640 V, 910.8 μ A cm ⁻² , 0.78)	2019, Hora et al. ¹⁷⁵
Co ³⁺ /Co ²⁺ (0.11 M [Co ³⁺ (bpy) ₃](PF ₆) ₃], (PF ₆) ₃ , 0.1 M LiClO ₄ , and 1.2 M TBP in MPN)	Y123	Pt	T5-fluorescent lamp	999.6 lx, $P_{in} = 311.47$ μ W cm ⁻²	24.5% (0.846 V, 1.24.38 μ A cm ⁻² , 0.725)	2019, Venkatesan et al. ¹⁷⁶
Cu ²⁺ /Cu ⁺ (0.04 M [Cu(tmby) ₂] ₂](TFSI) ₂ , 0.20 M [Cu(tmby) ₂] ₂](TFSI), 0.1 M LiTFSI and 0.6 M tributyl phosphate in ACN)	XY1 + D35 (organic, D-A- π -A, and D- π -A structure)	PEDOT	Osram 930 warm white fluorescent light	1000 lx, $P_{in} = 306.6$ μ W cm ⁻²	28.9% (0.797 V, 138 μ A cm ⁻² , 0.80)	2017, Freitag et al. ¹⁷⁷
Cu ²⁺ /Cu ⁺ (0.04 M [Cu(tmby) ₂] ₂](TFSI) ₂ , 0.20 M [Cu(tmby) ₂] ₂](TFSI), 0.1 M LiTFSI, and 0.6 M MBI in ACN)	Y123 + XY1b (organic D- π - π -A structure) + CDCA (coadsorbent)	PEDOT	Osram 930 warm white fluorescent light	1000 lx, $P_{in} = 318.2$ μ W cm ⁻²	31.8% (0.878 V, 0.418 mA, 0.773)	2018, Cao et al. ¹²
Cu ²⁺ /Cu ⁺ (0.2 M [Cu(tmby) ₂] ₂](TFSI) and 0.04 M [Cu(tmby) ₂] ₂](TFSI) ₂ , 0.1 M LiTFSI, and 0.6 M TBP in ACN)	XY1 + L1 (organic D-A- π -A and D- π -A structure) + CDCA (coadsorbent)	PEDOT	Osram 930 warm white fluorescent light	1000 lx, $P_{in} = 303.1$ μ W cm ⁻²	34.0% (0.910 V, 147 μ A cm ⁻² , 0.77)	2020, Michaels et al. ⁸¹
Cu ²⁺ /Cu ⁺ (0.1 M [Cu(tmby) ₂] ₂](TFSI), 0.04 M [Cu(tmby) ₂] ₂](TFSI) ₂ , 0.1 M LiTFSI, and 0.6 M MBI in ACN)	M55 + XY1b (organic D- π -A and D-A- π -A structure) + CDCA (coadsorbent)	PEDOT	Osram 930 warm white fluorescent light	1000 lx, $P_{in} = 318.2$ μ W cm ⁻²	34.5% (0.98 V, 0.387 mA, 0.815)	2021, Zhang et al. ⁸

Scheme 3. Proposed Strategy for the PCE Enhancement of over 16% in DSSCs under 1-Sun Illumination

1. Simultaneous Improvement of J_{sc} and V_{oc} by

- Redox shuttles with redox potential $\sim 0.45\text{--}0.65$ V vs NHE
- Co-sensitization of present dyes with NIR-absorbing dye



2. The improvement of FF by

- Using superior counter electrode, and
- Device optimization

0.3 V for dye regeneration, the use of a metal complex (especially, Co or Cu complexes) redox shuttle with redox potential of $\sim 0.45\text{--}0.65$ V may enhance the V_{oc} and J_{sc} values of the device simultaneously by reducing small potential loss and increasing the LHE. The proper optimization of the device and use of a superior catalyst for the specific redox shuttle can reduce the charge transfer resistances and enhance the fill factor of the devices.

In DSSC redox LEs, ACN-based solvents were highly effective; however, they are volatile. Ionic liquids can play a significant role as nonvolatile additives in the redox LEs to improve the stability of the device. The improvement of sealing by using advanced techniques and the development of semisolid electrolytes are also demanded for the long-term stability of the devices. Both TBP and MBI were effective as Lewis base additives in DSSC redox electrolytes; however, MBI was more effective for copper electrolytes than TBP. The additional coordination of Cu(II) complexes with the strong Lewis base TBP can slow down the reduction of Cu(II) species in the counter electrode, complicate the redox process, and negatively shift the redox potential. The record PCE of over 34% under ambient light was obtained by using a $[\text{Cu}(\text{tmby})_2]^{2+/+}$ complex redox shuttle, which ensures the great potential of copper-based redox electrolytes for commercial application in DSSCs to power IoT and low-power-consumption electronic devices.

AUTHOR INFORMATION

Corresponding Author

Hwan Kyu Kim – Global GET-Future Lab, Department of Advanced Materials Chemistry, Korea University, Sejong 339-700, Korea; orcid.org/0000-0002-6189-5237; Email: hkk777@korea.ac.kr

Author

Masud – Global GET-Future Lab, Department of Advanced Materials Chemistry, Korea University, Sejong 339-700, Korea; orcid.org/0000-0003-2397-6922

Complete contact information is available at:

<https://pubs.acs.org/10.1021/acsomega.2c06843>

Notes

The authors declare no competing financial interest.

ACKNOWLEDGMENTS

This work was supported by the Korean government (the Ministry of Science, ICT, and Future Planning) through the Midcareer Researcher Program (NRF-2021R1A2C2006328) and “Human Resources Program in Energy Technology” of the Korea Institute of Energy Technology Evaluation and Planning (KETEP), granted financial resources from the Ministry of Trade, Industry & Energy, Republic of Korea (KETEP-20204030200070).

REFERENCES

- (1) Perez, R.; Zweibel, K.; Hoff, T. E. Solar Power Generation in the US: Too Expensive, or a Bargain? *Energy Policy* **2011**, *39* (11), 7290–7297.
- (2) Launch of new RICOH EH DSSC modules with 20% increase in power generation | Global | Ricoh. https://www.ricoh.com/release/2021/0513_1/ (accessed 2021-05-31).
- (3) News - Exeger. <https://www.exeger.com/news/> (accessed 2021-08-11).
- (4) Kang, S. H.; Jeong, M. J.; Eom, Y. K.; Choi, I. T.; Kwon, S. M.; Yoo, Y.; Kim, J.; Kwon, J.; Park, J. H.; Kim, H. K. Porphyrin Sensitizers with Donor Structural Engineering for Superior Performance Dye-Sensitized Solar Cells and Tandem Solar Cells for Water Splitting Applications. *Adv. Energy Mater.* **2017**, *7* (7), 1602117.
- (5) Eom, Y. K.; Kang, S. H.; Choi, I. T.; Yoo, Y.; Kim, J.; Kim, H. K. Significant Light Absorption Enhancement by a Single Heterocyclic Unit Change in the π -Bridge Moiety from Thieno[3,2-b]-Benzothiophene to Thieno[3,2-b]Indole for High Performance Dye-Sensitized and Tandem Solar Cells. *J. Mater. Chem. A* **2017**, *5* (5), 2297–2308.
- (6) Eom, Y. K.; Choi, I. T.; Kang, S. H.; Lee, J.; Kim, J.; Ju, M. J.; Kim, H. K. Thieno[3,2-b][1]Benzothiophene Derivative as a New π -Bridge Unit in D- π -A Structural Organic Sensitizers with Over 10.47% Efficiency for Dye-Sensitized Solar Cells. *Adv. Energy Mater.* **2015**, *5* (15), 1500300.
- (7) Ji, J. M.; Zhou, H.; Kim, H. K. Rational Design Criteria for D- π -A Structured Organic and Porphyrin Sensitizers for Highly Efficient Dye-Sensitized Solar Cells. *J. Mater. Chem. A* **2018**, *6* (30), 14518–14545.
- (8) Zhang, D.; Stojanovic, M.; Ren, Y.; Cao, Y.; Eickemeyer, F. T.; Socie, E.; Vlachopoulos, N.; Moser, J.-E. E.; Zakeeruddin, S. M.; Hagfeldt, A.; Grätzel, M. A Molecular Photosensitizer Achieves a V_{oc} of 1.24 V Enabling Highly Efficient and Stable Dye-Sensitized Solar Cells with Copper(II/I)-Based Electrolyte. *Nat. Commun.* **2021**, *12* (1), 1777.
- (9) Ji, J. M.; Zhou, H.; Eom, Y. K.; Kim, C. H.; Kim, H. K. 14.2% Efficiency Dye-Sensitized Solar Cells by Co-Sensitizing Novel Thieno[3,2-b]Indole-Based Organic Dyes with a Promising Porphyrin Sensitizer. *Adv. Energy Mater.* **2020**, *10* (15), 2000124.
- (10) Zeng, K.; Chen, Y.; Zhu, W. H.; Tian, H.; Xie, Y. Efficient Solar Cells Based on Concerted Companion Dyes Containing Two Complementary Components: An Alternative Approach for Cosensitization. *J. Am. Chem. Soc.* **2020**, *142* (11), 5154–5161.
- (11) Kakiage, K.; Aoyama, Y.; Yano, T.; Oya, K.; Fujisawa, J. I.; Hanaya, M. Highly-Efficient Dye-Sensitized Solar Cells with Collaborative Sensitization by Silyl-Anchor and Carboxy-Anchor Dyes. *Chem. Commun.* **2015**, *51* (88), 15894–15897.
- (12) Cao, Y.; Liu, Y.; Zakeeruddin, S. M.; Hagfeldt, A.; Grätzel, M. Direct Contact of Selective Charge Extraction Layers Enables High-Efficiency Molecular Photovoltaics. *Joule* **2018**, *2* (6), 1108–1117.
- (13) Daenke, T.; Kwon, T. H.; Holmes, A. B.; Duffy, N. W.; Bach, U.; Spiccia, L. High-Efficiency Dye-Sensitized Solar Cells with Ferrocene-Based Electrolytes. *Nat. Chem.* **2011**, *3* (3), 211–215.
- (14) Hattori, S.; Wada, Y.; Yanagida, S.; Fukuzumi, S. Blue Copper Model Complexes with Distorted Tetragonal Geometry Acting as Effective Electron-Transfer Mediators in Dye-Sensitized Solar Cells. *J. Am. Chem. Soc.* **2005**, *127* (26), 9648–9654.

- (15) Feldt, S. M.; Gibson, E. A.; Gabriellson, E.; Sun, L.; Boschloo, G.; Hagfeldt, A. Design of Organic Dyes and Cobalt Polypyridine Redox Mediators for High-Efficiency Dye-Sensitized Solar Cells. *J. Am. Chem. Soc.* **2010**, *132* (46), 16714–16724.
- (16) Saygili, Y.; Söderberg, M.; Pellet, N.; Giordano, F.; Cao, Y.; Munoz-García, A. B.; Zakeeruddin, S. M.; Vlachopoulos, N.; Pavone, M.; Boschloo, G.; Kavan, L.; Moser, J. E.; Grätzel, M.; Hagfeldt, A.; Freitag, M. Copper Bipyridyl Redox Mediators for Dye-Sensitized Solar Cells with High Photovoltage. *J. Am. Chem. Soc.* **2016**, *138* (45), 15087–15096.
- (17) Yang, W.; Vlachopoulos, N.; Hao, Y.; Hagfeldt, A.; Boschloo, G. Efficient Dye Regeneration at Low Driving Force Achieved in Triphenylamine Dye LEG4 and TEMPO Redox Mediator Based Dye-Sensitized Solar Cells. *Phys. Chem. Chem. Phys.* **2015**, *17* (24), 15868–15875.
- (18) Zhang, Z.; Chen, P.; Murakami, T. N.; Zakeeruddin, S. M.; Grätzel, M. The 2,2,6,6-Tetramethyl-1-Piperidinyloxy Radical: An Efficient, Iodine-Free Redox Mediator for Dye-Sensitized Solar Cells. *Adv. Funct. Mater.* **2008**, *18* (2), 341–346.
- (19) Masud; Kim, K. M.; Kim, H. K. Highly Efficient Gel Electrolytes by End Group Modified PEG-Based ABA Triblock Copolymers for Quasi-Solid-State Dye-Sensitized Solar Cells. *Chem. Eng. J.* **2021**, *420*, 129899.
- (20) Suzuka, M.; Hayashi, N.; Sekiguchi, T.; Sumioka, K.; Takata, M.; Hayo, N.; Ikeda, H.; Oyaizu, K.; Nishide, H. A Quasi-Solid State DSSC with 10.1% Efficiency through Molecular Design of the Charge-Separation and -Transport. *Sci. Rep.* **2016**, *6* (June), 1–7.
- (21) Chen, C.-L.; Chang, T.-W.; Teng, H.; Wu, C.-G.; Chen, C.-Y.; Yang, Y.-M.; Lee, Y.-L. Highly Efficient Gel-State Dye-Sensitized Solar Cells Prepared Using Poly(Acrylonitrile-Co-Vinyl Acetate) Based Polymer Electrolytes. *Phys. Chem. Chem. Phys.* **2013**, *15* (10), 3640–3645.
- (22) Jeon, I.-Y.; Kim, H. M.; Kweon, D. H.; Jung, S.-M.; Seo, J.-M.; Shin, S.-H.; Choi, I. T.; Eom, Y. K.; Kang, S. H.; Kim, H. K.; Ju, M. J.; Baek, J.-B. Metalloid Tellurium-Doped Graphene Nanoplatelets as Ultimately Stable Electrocatalysts for Cobalt Reduction Reaction in Dye-Sensitized Solar Cells. *Nano Energy* **2016**, *30*, 867–876.
- (23) Ju, M. J.; Jeon, I.-Y.; Kim, H. M.; Choi, J. I.; Jung, S.-M.; Seo, J.-M.; Choi, I. T.; Kang, S. H.; Kim, H. S.; Noh, M. J.; Lee, J.-J.; Jeong, H. Y.; Kim, H. K.; Kim, Y.-H.; Baek, J.-B. Edge-Selenated Graphene Nanoplatelets as Durable Metal-Free Catalysts for Iodine Reduction Reaction in Dye-Sensitized Solar Cells. *Sci. Adv.* **2016**, *2* (6), e1501459.
- (24) Ju, M. J.; Jeon, I.-Y.; Kim, J. C.; Lim, K.; Choi, H.-J.; Jung, S.-M.; Choi, I. T.; Eom, Y. K.; Kwon, Y. J.; Ko, J.; Lee, J.-J.; Kim, H. K.; Baek, J.-B. Graphene Nanoplatelets Doped with N at Its Edges as Metal-Free Cathodes for Organic Dye-Sensitized Solar Cells. *Adv. Mater.* **2014**, *26* (19), 3055–3062.
- (25) Ju, M. J.; Jeon, I.-Y.; Lim, K.; Kim, J. C.; Choi, H.-J.; Choi, I. T.; Eom, Y. K.; Kwon, Y. J.; Ko, J.; Lee, J.-J.; Baek, J.-B.; Kim, H. K. Edge-Carboxylated Graphene Nanoplatelets as Oxygen-Rich Metal-Free Cathodes for Organic Dye-Sensitized Solar Cells. *Energy Environ. Sci.* **2014**, *7* (3), 1044–1052.
- (26) Ellis, H.; Vlachopoulos, N.; Häggman, L.; Perruchot, C.; Jouini, M.; Boschloo, G.; Hagfeldt, A. PEDOT Counter Electrodes for Dye-Sensitized Solar Cells Prepared by Aqueous Micellar Electrodeposition. *Electrochim. Acta* **2013**, *107*, 45–51.
- (27) Aftabuzzaman, M.; Lu, C.; Kim, H. K. Recent Progress on Nanostructured Carbon-Based Counter/Back Electrodes for High-Performance Dye-Sensitized and Perovskite Solar Cells. *Nanoscale* **2020**, *12* (34), 17590–17648.
- (28) Zou, J.; Wang, Y.; Baryshnikov, G.; Luo, J.; Wang, X.; Ågren, H.; Li, C.; Xie, Y. Efficient Dye-Sensitized Solar Cells Based on a New Class of Doubly Concerted Companion Dyes. *ACS Appl. Mater. Interfaces* **2022**, *14* (29), 33274–33284.
- (29) Ren, Y.; Zhang, D.; Suo, J.; Cao, Y.; Eickemeyer, F. T.; Vlachopoulos, N.; Zakeeruddin, S. M.; Hagfeldt, A.; Grätzel, M. Hydroxamic Acid Preadsorption Raises Efficiency of Cosensitized Solar Cells. *Nature* **2023**, *613*, 60.
- (30) Higashino, T.; Imahori, H. Emergence of Copper(I/II) Complexes as Third-Generation Redox Shuttles for Dye-Sensitized Solar Cells. *ACS Energy Lett.* **2022**, *7* (6), 1926–1938.
- (31) Sastrawan, R.; Beier, J.; Belledin, U.; Hemming, S.; Hinsch, A.; Kern, R.; Vetter, C.; Petrat, F. M.; Prodi-Schwab, A.; Lechner, P.; Hoffmann, W. A Glass Frit-Sealed Dye Solar Cell Module with Integrated Series Connections. *Sol. Energy Mater. Sol. Cells* **2006**, *90* (11), 1680–1691.
- (32) Martins, J.; Emami, S.; Ivanou, D.; Mendes, A. Ultralow Temperature Glass Frit Encapsulation for Stable Dye-Sensitized Solar Cells. *ACS Appl. Energy Mater.* **2022**, *5* (11), 14185–14192.
- (33) Masud; Kim, K. M.; Kim, H. K. Polymer Gel Electrolytes Based on PEG-Functionalized ABA Triblock Copolymers for Quasi-Solid-State Dye-Sensitized Solar Cells: Molecular Engineering and Key Factors. *ACS Appl. Mater. Interfaces* **2020**, *12* (37), 42067–42080.
- (34) Hagfeldt, A.; Boschloo, G.; Sun, L.; Kloo, L.; Pettersson, H. Dye-Sensitized Solar Cells. *Chem. Rev.* **2010**, *110* (11), 6595–6663.
- (35) Sun, C.; Li, Y.; Song, P.; Ma, F. An Experimental and Theoretical Investigation of the Electronic Structures and Photoelectrical Properties of Ethyl Red and Carminic Acid for DSSC Application. *Materials (Basel)*. **2016**, *9* (10), 813.
- (36) Ardo, S.; Meyer, G. J. Photodriven Heterogeneous Charge Transfer with Transition-Metal Compounds Anchored to TiO₂ Semiconductor Surfaces. *Chem. Soc. Rev.* **2009**, *38* (1), 115–164.
- (37) Katoh, R.; Furube, A. Electron Injection Efficiency in Dye-Sensitized Solar Cells. *J. Photochem. Photobiol. C Photochem. Rev.* **2014**, *20*, 1–16.
- (38) Zhang, S.; Yang, X.; Numata, Y.; Han, L. Highly Efficient Dye-Sensitized Solar Cells: Progress and Future Challenges. *Energy Environ. Sci.* **2013**, *6* (6), 1443–1464.
- (39) Bisquert, J.; Zaban, A.; Salvador, P. Analysis of the Mechanisms of Electron Recombination in Nanoporous TiO₂ Dye-Sensitized Solar Cells. Nonequilibrium Steady-State Statistics and Interfacial Electron Transfer via Surface States. *J. Phys. Chem. B* **2002**, *106* (34), 8774–8782.
- (40) Zaban, A.; Greenshtein, M.; Bisquert, J. Determination of the Electron Lifetime in Nanocrystalline Dye Solar Cells by Open-Circuit Voltage Decay Measurements. *ChemPhysChem* **2003**, *4* (8), 859–864.
- (41) Nazeeruddin, M. K.; Baranoff, E.; Grätzel, M. Dye-Sensitized Solar Cells: A Brief Overview. *Sol. Energy* **2011**, *85* (6), 1172–1178.
- (42) Aftabuzzaman, M.; Sarker, S.; Lu, C.; Kim, H. K. In-Depth Understanding of the Energy Loss and Efficiency Limit of Dye-Sensitized Solar Cells under Outdoor and Indoor Conditions. *J. Mater. Chem. A* **2021**, *9* (44), 24830–24848.
- (43) Liu, X.; Zhang, Q.; Li, J.; Valanoor, N.; Tang, X.; Cao, G. Increase of Power Conversion Efficiency in Dye-Sensitized Solar Cells through Ferroelectric Substrate Induced Charge Transport Enhancement. *Sci. Rep.* **2018**, *8* (1), 17389.
- (44) Wang, M.; Grätzel, C.; Zakeeruddin, S. M.; Grätzel, M. Recent Developments in Redox Electrolytes for Dye-Sensitized Solar Cells. *Energy Environ. Sci.* **2012**, *5* (11), 9394–9405.
- (45) Benesperi, I.; Michaels, H.; Freitag, M. The Researcher's Guide to Solid-State Dye-Sensitized Solar Cells. *J. Mater. Chem. C* **2018**, *6* (44), 11903–11942.
- (46) Ma, P.; Fang, Y.; Li, A.; Wen, B.; Cheng, H.; Zhou, X.; Shi, Y.; Yang, H. Y.; Lin, Y. Highly Efficient and Stable Ionic Liquid-Based Gel Electrolytes. *Nanoscale* **2021**, *13* (15), 7140–7151.
- (47) Saidi, N. M.; Omar, F. S.; Numan, A.; Apperley, D. C.; Algaradah, M. M.; Kasi, R.; Avestro, A.-J.; Subramaniam, R. T. Enhancing the Efficiency of a Dye-Sensitized Solar Cell Based on a Metal Oxide Nanocomposite Gel Polymer Electrolyte. *ACS Appl. Mater. Interfaces* **2019**, *11* (33), 30185–30196.
- (48) Bard, J. A.; Faulkner, L. R. *Electrochemical Methods: Fundamentals and Applications*, 2nd ed.; Wiley: 2000.
- (49) Owen, J. Ionic Conductivity. In *Comprehensive Polymer Science and Supplements*; Elsevier: 1989; pp 669–686. DOI: 10.1016/b978-0-08-096701-1.00058-6.
- (50) Ratner, M. A.; Shriver, D. F. Ion Transport in Solvent-Free Polymers. *Chem. Rev.* **1988**, *88* (1), 109–124.

- (51) Menzinger, M.; Wolfgang, R. The Meaning and Use of the Arrhenius Activation Energy. *Angew. Chem., Int. Ed. Engl.* **1969**, *8* (6), 438–444.
- (52) Arrhenius, S. Über Die Reaktionsgeschwindigkeit Bei Der Inversion von Rohrzucker Durch Säuren. *Zeitschrift für Phys. Chemie* **1889**, *4U* (1), 226–248.
- (53) Bandara, T. M. W. J.; Senavirathna, S. L. N.; Wickramasinghe, H. M. N.; Vignarooban, K.; De Silva, L. A.; Dissanayake, M. A. K. L.; Albinsson, I.; Mellander, B. Binary Counter Ion Effects and Dielectric Behavior of Iodide Ion Conducting Gel-Polymer Electrolytes for High-Efficiency Quasi-Solid-State Solar Cells. *Phys. Chem. Chem. Phys.* **2020**, *22* (22), 12532–12543.
- (54) Vogel, H. Das Temperaturabhängigkeitsgesetz Der Viskosität von Flüssigkeiten. *Phys. Zeitschrift* **1921**, *22*, 645.
- (55) Fulcher, G. S. ANALYSIS OF RECENT MEASUREMENTS OF THE VISCOSITY OF GLASSES. *J. Am. Ceram. Soc.* **1925**, *8* (6), 339–355.
- (56) Tammann, G.; Hesse, W. Die Abhängigkeit Der Viskosität von Der Temperatur Bie Unterkühlten Flüssigkeiten. *Zeitschrift für Anorg. und Allg. Chemie* **1926**, *156* (1), 245–257.
- (57) Dahms, H. Electronic Conduction in Aqueous Solution. *J. Phys. Chem.* **1968**, *72* (1), 362–364.
- (58) Ruff, I.; Friedrich, V. J. Transfer Diffusion. I. Theoretical. *J. Phys. Chem.* **1971**, *75* (21), 3297–3302.
- (59) Tahara, H.; Tanaka, Y.; Yamamoto, S.; Yonemori, S.; Chan, B.; Murakami, H.; Sagara, T. A Redox-Active Ionic Liquid Manifesting Charge-Transfer Interaction between a Viologen and Carbazole and Its Effect on the Viscosity, Ionic Conductivity, and Redox Process of the Viologen. *Chem. Sci.* **2021**, *12* (13), 4872–4882.
- (60) Sun, H.; Zhang, L.; Wang, Z.-S. Single-Crystal CoSe₂ Nanorods as an Efficient Electrocatalyst for Dye-Sensitized Solar Cells. *J. Mater. Chem. A* **2014**, *2* (38), 16023–16029.
- (61) Hauch, A.; Georg, A. Diffusion in the Electrolyte and Charge-Transfer Reaction at the Platinum Electrode in Dye-Sensitized Solar Cells. *Electrochim. Acta* **2001**, *46* (22), 3457–3466.
- (62) Girma, W. M.; Chen, C. H.; Yang, C. H.; Wang, P. I.; Ou, K. L.; Liaw, D. J.; Chang, J. Y. A Low Molecular Mass Organogelator Electrolyte with TiO₂ Nanoparticles for Stable and Efficient Quasi-Solid-State Dye Sensitized Solar Cells. *RSC Adv.* **2017**, *7* (13), 7671–7678.
- (63) Papageorgiou, N.; Athanassov, Y.; Armand, M.; Bonhote, P.; Pettersson, H.; Azam, A.; Grätzel, M. The Performance and Stability of Ambient Temperature Molten Salts for Solar Cell Applications. *J. Electrochem. Soc.* **1996**, *143* (10), 3099–3108.
- (64) Chatzivasiloglou, E.; Stergiopoulos, T.; Kontos, A. G.; Alexis, N.; Prodromidis, M.; Falaras, P. The Influence of the Metal Cation and the Filler on the Performance of Dye-Sensitized Solar Cells Using Polymer-Gel Redox Electrolytes. *J. Photochem. Photobiol. A Chem.* **2007**, *192* (1), 49–55.
- (65) Boschloo, G.; Hagfeldt, A. Characteristics of the Iodide/Triiodide Redox Mediator in Dye-Sensitized Solar Cells. *Acc. Chem. Res.* **2009**, *42* (11), 1819–1826.
- (66) O'Regan, B.; Grätzel, M. A Low-Cost, High-Efficiency Solar Cell Based on Dye-Sensitized Colloidal TiO₂ Films. *Nature* **1991**, *353* (6346), 737–740.
- (67) Chen, C.-Y.; Wang, M.; Li, J.-Y.; Pootrakulchote, N.; Alibabaei, L.; Ngoc-le, C.; Decoppet, J.-D.; Tsai, J.-H.; Grätzel, C.; Wu, C.-G.; Zakeeruddin, S. M.; Grätzel, M. Highly Efficient Light-Harvesting Ruthenium Sensitizer for Thin-Film Dye-Sensitized Solar Cells. *ACS Nano* **2009**, *3* (10), 3103–3109.
- (68) Yu, Q.; Wang, Y.; Yi, Z.; Zu, N.; Zhang, J.; Zhang, M.; Wang, P. High-Efficiency Dye-Sensitized Solar Cells: The Influence of Lithium Ions on Exciton Dissociation, Charge Recombination, and Surface States. *ACS Nano* **2010**, *4* (10), 6032–6038.
- (69) Han, L.; Islam, A.; Chen, H.; Malapaka, C.; Chiranjeevi, B.; Zhang, S.; Yang, X.; Yanagida, M. High-Efficiency Dye-Sensitized Solar Cell with a Novel Co-Adsorbent. *Energy Environ. Sci.* **2012**, *5* (3), 6057–6060.
- (70) Zhou, D.; Xia, Z.; Shang, H.; Xiao, H.; Jiang, Z.; Li, H.; Zheng, L.; Dong, J.; Chen, W. A Rational Design of an Efficient Counter Electrode with the Co/Co₁P₁N₃ Atomic Interface for Promoting Catalytic Performance. *Mater. Chem. Front.* **2021**, *5* (7), 3085–3092.
- (71) Wang, Q.; Ito, S.; Grätzel, M.; Fabregat-Santiago, F.; Mora-Seró, I.; Bisquert, J.; Bessho, T.; Imai, H. Characteristics of High Efficiency Dye-Sensitized Solar Cells. *J. Phys. Chem. B* **2006**, *110* (50), 25210–25221.
- (72) Nazeeruddin, M. K.; Kay, A.; Rodicio, I.; Humphry-Baker, R.; Mueller, E.; Liska, P.; Vlachopoulos, N.; Graetzel, M. Conversion of Light to Electricity by Cis-X₂bis(2,2'-Bipyridyl-4,4'-Dicarboxylate)-Ruthenium(II) Charge-Transfer Sensitizers (X = Cl-, Br-, I-, CN-, and SCN-) on Nanocrystalline Titanium Dioxide Electrodes. *J. Am. Chem. Soc.* **1993**, *115* (14), 6382–6390.
- (73) Wang, Z.-S.; Sayama, K.; Sugihara, H. Efficient Eosin Y Dye-Sensitized Solar Cell Containing Br-/Br₃- Electrolyte. *J. Phys. Chem. B* **2005**, *109* (47), 22449–22455.
- (74) Teng, C.; Yang, X.; Yuan, C.; Li, C.; Chen, R.; Tian, H.; Li, S.; Hagfeldt, A.; Sun, L. Two Novel Carbazole Dyes for Dye-Sensitized Solar Cells with Open-Circuit Voltages up to 1 V Based on Br-/Br₃- Electrolytes. *Org. Lett.* **2009**, *11* (23), 5542–5545.
- (75) Wang, P.; Zakeeruddin, S. M.; Moser, J.-E.; Humphry-Baker, R.; Grätzel, M. A Solvent-Free, SeCN⁻/(SeCN)₃- Based Ionic Liquid Electrolyte for High-Efficiency Dye-Sensitized Nanocrystalline Solar Cells. *J. Am. Chem. Soc.* **2004**, *126* (23), 7164–7165.
- (76) Oskam, G.; Bergeron, B. V.; Meyer, G. J.; Searson, P. C. Pseudohalogens for Dye-Sensitized TiO₂ Photoelectrochemical Cells. *J. Phys. Chem. B* **2001**, *105* (29), 6867–6873.
- (77) Zhou, H.; Ji, J.-M.; Kang, S. H.; Kim, M. S.; Lee, H. S.; Kim, C. H.; Kim, H. K. Molecular Design and Synthesis of D-π-A Structured Porphyrin Dyes with Various Acceptor Units for Dye-Sensitized Solar Cells. *J. Mater. Chem. C* **2019**, *7* (10), 2843–2852.
- (78) Yum, J.-H.; Baranoff, E.; Kessler, F.; Moehl, T.; Ahmad, S.; Bessho, T.; Marchioro, A.; Ghadiri, E.; Moser, J.-E.; Yi, C.; Nazeeruddin, M. K.; Grätzel, M. A Cobalt Complex Redox Shuttle for Dye-Sensitized Solar Cells with High Open-Circuit Potentials. *Nat. Commun.* **2012**, *3* (1), 1–8.
- (79) Yella, A.; Lee, H.-W. W.; Tsao, H. N.; Yi, C.; Chandiran, A. K.; Nazeeruddin, M. K. K.; Diau, E. W.-G. G.; Yeh, C.-Y. Y.; Zakeeruddin, S. M.; Grätzel, M. Porphyrin-Sensitized Solar Cells with Cobalt (II/III)-Based Redox Electrolyte Exceed 12% Efficiency. *Science* (80-) **2011**, *334* (6056), 629–634.
- (80) Ren, Y.; Sun, D.; Cao, Y.; Tsao, H. N.; Yuan, Y.; Zakeeruddin, S. M.; Wang, P.; Grätzel, M. A Stable Blue Photosensitizer for Color Palette of Dye-Sensitized Solar Cells Reaching 12.6% Efficiency. *J. Am. Chem. Soc.* **2018**, *140* (7), 2405–2408.
- (81) Michaels, H.; Rinderle, M.; Freitag, R.; Benesperi, I.; Edvinsson, T.; Socher, R.; Gagliardi, A.; Freitag, M. Dye-Sensitized Solar Cells under Ambient Light Powering Machine Learning: Towards Autonomous Smart Sensors for the Internet of Things. *Chem. Sci.* **2020**, *11* (11), 2895–2906.
- (82) Cong, J.; Kinschel, D.; Daniel, Q.; Safdari, M.; Gabrielson, E.; Chen, H.; Svensson, P. H.; Sun, L.; Kloo, L. Bis(1,1-Bis(2-Pyridyl)Ethane)Copper(I/II) as an Efficient Redox Couple for Liquid Dye-Sensitized Solar Cells. *J. Mater. Chem. A* **2016**, *4* (38), 14550–14554.
- (83) Bai, Y.; Yu, Q.; Cai, N.; Wang, Y.; Zhang, M.; Wang, P. High-Efficiency Organic Dye-Sensitized Mesoscopic Solar Cells with a Copper Redox Shuttle. *Chem. Commun.* **2011**, *47* (15), 4376–4378.
- (84) Rodrigues, R. R.; Peddapuram, A.; Dorris, A. L.; Hammer, N. I.; Delcamp, J. H. Thienopyrroledione-Based Photosensitizers as Strong Photoinduced Oxidants: Oxidation of Fe(Bpy)₃²⁺ in a > 1.3 V Dye-Sensitized Solar Cell. *ACS Appl. Energy Mater.* **2019**, *2* (8), 5547–5556.
- (85) Curiac, C.; Rodrigues, R. R.; Watson, J.; Hunt, L. A.; Devdass, A.; Jurss, J. W.; Hammer, N. I.; Fortenberry, R. C.; Delcamp, J. H. Iron Redox Shuttles with Wide Optical Gap Dyes for High-Voltage Dye-Sensitized Solar Cells. *ChemSusChem* **2021**, *14*, 3084.

- (86) Hamann, T. W.; Farha, O. K.; Hupp, J. T. Outer-Sphere Redox Couples as Shuttles in Dye-Sensitized Solar Cells. Performance Enhancement Based on Photoelectrode Modification via Atomic Layer Deposition. *J. Phys. Chem. C* **2008**, *112* (49), 19756–19764.
- (87) Zhang, Z.; Chen, P.; Murakami, T. N.; Zakeeruddin, S. M.; Grätzel, M. The 2,2,6,6-Tetramethyl-1-Piperidinyloxy Radical: An Efficient, Iodine-Free Redox Mediator for Dye-Sensitized Solar Cells. *Adv. Funct. Mater.* **2008**, *18* (2), 341–346.
- (88) Wang, M.; Chamberland, N.; Breaux, L.; Moser, J.-E.; Humphry-Baker, R.; Marsan, B.; Zakeeruddin, S. M.; Grätzel, M. An Organic Redox Electrolyte to Rival Triiodide/Iodide in Dye-Sensitized Solar Cells. *Nat. Chem.* **2010**, *2* (5), 385–389.
- (89) Daeneke, T.; Mozer, A. J.; Kwon, T. H.; Duffy, N. W.; Holmes, A. B.; Bach, U.; Spiccia, L. Dye Regeneration and Charge Recombination in Dye-Sensitized Solar Cells with Ferrocene Derivatives as Redox Mediators. *Energy Environ. Sci.* **2012**, *5* (5), 7090–7099.
- (90) Daeneke, T.; Mozer, A. J.; Uemura, Y.; Makuta, S.; Fekete, M.; Tachibana, Y.; Koumura, N.; Bach, U.; Spiccia, L. Dye Regeneration Kinetics in Dye-Sensitized Solar Cells. *J. Am. Chem. Soc.* **2012**, *134* (41), 16925–16928.
- (91) Tian, H.; Jiang, X.; Yu, Z.; Kloo, L.; Hagfeldt, A.; Sun, L. Efficient Organic-Dye-Sensitized Solar Cells Based on an Iodine-Free Electrolyte. *Angew. Chemie Int. Ed.* **2010**, *49* (40), 7328–7331.
- (92) Okada, K.; Matsui, H.; Kawashima, T.; Ezure, T.; Tanabe, N. 100 Mm × 100 Mm Large-Sized Dye Sensitized Solar Cells. *J. Photochem. Photobiol. A Chem.* **2004**, *164* (1–3), 193–198.
- (93) Yu, Z.; Vlachopoulos, N.; Gorlov, M.; Kloo, L. Liquid Electrolytes for Dye-Sensitized Solar Cells. *Dalt. Trans.* **2011**, *40* (40), 10289–10303.
- (94) Pavlishchuk, V. V.; Addison, A. W. Conversion Constants for Redox Potentials Measured versus Different Reference Electrodes in Acetonitrile Solutions at 25°C. *Inorg. Chim. Acta* **2000**, *298* (1), 97–102.
- (95) Brown, K. N.; Gulyas, P. T.; Lay, P. A.; McAlpine, N. S.; Masters, A. F.; Phillips, L. Electrochemistry of Chlorinated Ferrocenes: Stability of Chlorinated Ferrocenium Ions. *J. Chem. Soc. Dalt. Trans.* **1993**, *6*, 835–840.
- (96) Noviadri, I.; Brown, K. N.; Fleming, D. S.; Gulyas, P. T.; Lay, P. A.; Masters, A. F.; Phillips, L. The Decamethylferrocenium/Decamethylferrocene Redox Couple: A Superior Redox Standard to the Ferrocenium/Ferrocene Redox Couple for Studying Solvent Effects on the Thermodynamics of Electron Transfer. *J. Phys. Chem. B* **1999**, *103* (32), 6713–6722.
- (97) Rodrigues, R. R.; Cheema, H.; Delcamp, J. H. A High-Voltage Molecular-Engineered Organic Sensitizer–Iron Redox Shuttle Pair: 1.4 V DSSC and 3.3 V SSM-DSSC Devices. *Angew. Chemie - Int. Ed.* **2018**, *57* (19), 5472–5476.
- (98) Spokoyny, A. M.; Li, T. C.; Farha, O. K.; Machan, C. W.; She, C.; Stern, C. L.; Marks, T. J.; Hupp, J. T.; Mirkin, C. A. Electronic Tuning of Nickel-Based Bis(Dicarbollide) Redox Shuttles in Dye-Sensitized Solar Cells. *Angew. Chemie Int. Ed.* **2010**, *49* (31), 5339–5343.
- (99) Perera, I. R.; Gupta, A.; Xiang, W.; Daeneke, T.; Bach, U.; Evans, R. A.; Ohlin, C. A.; Spiccia, L. Introducing Manganese Complexes as Redox Mediators for Dye-Sensitized Solar Cells. *Phys. Chem. Chem. Phys.* **2014**, *16* (24), 12021–12028.
- (100) Mosconi, E.; Yum, J.-H.; Kessler, F.; Gómez García, C. J.; Zuccaccia, C.; Cinti, A.; Nazeeruddin, M. K.; Grätzel, M.; De Angelis, F. Cobalt Electrolyte/Dye Interactions in Dye-Sensitized Solar Cells: A Combined Computational and Experimental Study. *J. Am. Chem. Soc.* **2012**, *134* (47), 19438–19453.
- (101) Nusbaumer, H.; Zakeeruddin, S. M.; Moser, J.-E. E.; Grätzel, M. An Alternative Efficient Redox Couple for the Dye-Sensitized Solar Cell System. *Chem. - Eur. J.* **2003**, *9* (16), 3756–3763.
- (102) Nusbaumer, H.; Moser, J.-E. E.; Zakeeruddin, S. M.; Nazeeruddin, M. K.; Grätzel, M. CoII(Dbip)2⁺ Complex Rivals Tri-Iodide/Iodide Redox Mediator in Dye-Sensitized Photovoltaic Cells. *J. Phys. Chem. B* **2001**, *105* (43), 10461–10464.
- (103) Wang, H.; Nicholson, P. G.; Peter, L.; Zakeeruddin, S. M.; Grätzel, M. Transport and Interfacial Transfer of Electrons in Dye-Sensitized Solar Cells Utilizing a Co(Dbip)2 Redox Shuttle. *J. Phys. Chem. C* **2010**, *114* (33), 14300–14306.
- (104) Song, B. J.; Song, H. M.; Choi, I. T.; Kim, S. K.; Seo, K. D.; Kang, M. S.; Lee, M. J.; Cho, D. W.; Ju, M. J.; Kim, H. K. A Desirable Hole-Conducting Coadsorbent for Highly Efficient Dye-Sensitized Solar Cells through an Organic Redox Cascade Strategy. *Chem. - A Eur. J.* **2011**, *17* (40), 11115–11121.
- (105) Mathew, S.; Yella, A.; Gao, P.; Humphry-Baker, R.; Curchod, B. F. E.; Ashari-Astani, N.; Tavernelli, L.; Rothlisberger, U.; Nazeeruddin, M. K.; Grätzel, M. Dye-Sensitized Solar Cells with 13% Efficiency Achieved through the Molecular Engineering of Porphyrin Sensitizers. *Nat. Chem.* **2014**, *6* (3), 242–247.
- (106) Kavan, L.; Saygili, Y.; Freitag, M.; Zakeeruddin, S. M.; Hagfeldt, A.; Grätzel, M. Electrochemical Properties of Cu(II/I)-Based Redox Mediators for Dye-Sensitized Solar Cells. *Electrochim. Acta* **2017**, *227*, 194–202.
- (107) Cao, Y.; Saygili, Y.; Ummadisingu, A.; Teuscher, J.; Luo, J.; Pellet, N.; Giordano, F.; Zakeeruddin, S. M.; Moser, J.-E.; Freitag, M.; Hagfeldt, A.; Grätzel, M. 11% Efficiency Solid-State Dye-Sensitized Solar Cells with Copper(II/I) Hole Transport Materials. *Nat. Commun.* **2017**, *8* (1), 15390.
- (108) Pradhan, S. C.; Hagfeldt, A.; Soman, S. Resurgence of DSCs with Copper Electrolyte: A Detailed Investigation of Interfacial Charge Dynamics with Cobalt and Iodine Based Electrolytes. *J. Mater. Chem. A* **2018**, *6* (44), 22204–22214.
- (109) Davies, K.; Byers, B. Kinetic Study of Electron-Transfer of Sterically Constrained Bis(Diimine) Complexes of Copper(II) and Copper (I) with Ruthenium Ammine Complexes. *Inorg. Chem.* **1987**, *26* (22), 3823–3825.
- (110) Cazzanti, S.; Caramori, S.; Argazzi, R.; Elliott, C. M.; Bignozzi, C. A. Efficient Non-Corrosive Electron-Transfer Mediator Mixtures for Dye-Sensitized Solar Cells. *J. Am. Chem. Soc.* **2006**, *128* (31), 9996–9997.
- (111) Liu, J.; Yang, X.; Cong, J.; Kloo, L.; Sun, L. Solvent-Free Ionic Liquid Electrolytes without Elemental Iodine for Dye-Sensitized Solar Cells. *Phys. Chem. Chem. Phys.* **2012**, *14* (33), 11592–11595.
- (112) Chu, T.-C.; Lin, R. Y.-Y.; Lee, C.-P.; Hsu, C.-Y.; Shih, P.-C.; Lin, R.; Li, S.-R.; Sun, S.-S.; Lin, J. T.; Vittal, R.; Ho, K.-C. Ionic Liquid with a Dual-Redox Couple for Efficient Dye-Sensitized Solar Cells. *ChemSusChem* **2014**, *7* (1), 146–153.
- (113) Cong, J.; Hao, Y.; Boschloo, G.; Kloo, L. Electrolytes Based on TEMPO–Co Tandem Redox Systems Outperform Single Redox Systems in Dye-Sensitized Solar Cells. *ChemSusChem* **2015**, *8* (2), 264–268.
- (114) Hao, Y.; Yang, W.; Karlsson, M.; Cong, J.; Wang, S.; Li, X.; Xu, B.; Hua, J.; Kloo, L.; Boschloo, G. Efficient Dye-Sensitized Solar Cells with Voltages Exceeding 1 V through Exploring Tris(4-Alkoxyphenyl)Amine Mediators in Combination with the Tris(Bipyridine) Cobalt Redox System. *ACS Energy Lett.* **2018**, *3* (8), 1929–1937.
- (115) Mariotti, N.; Bonomo, M.; Fagiolarì, L.; Barbero, N.; Gerbaldi, C.; Bella, F.; Barolo, C. Recent Advances in Eco-Friendly and Cost-Effective Materials towards Sustainable Dye-Sensitized Solar Cells. *Green Chem.* **2020**, *22* (21), 7168–7218.
- (116) Law, C.; Pathirana, S. C.; Li, X.; Anderson, A. Y.; Barnes, P. R. F.; Listorti, A.; Ghaddar, T. H.; O'Regan, B. C. Water-Based Electrolytes for Dye-Sensitized Solar Cells. *Adv. Mater.* **2010**, *22* (40), 4505–4509.
- (117) Bella, F.; Galliano, S.; Falco, M.; Viscardi, G.; Barolo, C.; Grätzel, M.; Gerbaldi, C. Approaching Truly Sustainable Solar Cells by the Use of Water and Cellulose Derivatives. *Green Chem.* **2017**, *19* (4), 1043–1051.
- (118) Bella, F.; Porcarelli, L.; Mantione, D.; Gerbaldi, C.; Barolo, C.; Grätzel, M.; Mecerreyes, D. A Water-Based and Metal-Free Dye Solar Cell Exceeding 7% Efficiency Using a Cationic Poly(3,4-Ethylene-dioxythiophene) Derivative. *Chem. Sci.* **2020**, *11* (6), 1485–1493.

- (119) Tributsch, H. Dye Sensitization Solar Cells: A Critical Assessment of the Learning Curve. *Coord. Chem. Rev.* **2004**, *248* (13–14), 1511–1530.
- (120) Yang, W.; Söderberg, M.; Eriksson, A. I. K.; Boschloo, G. Efficient Aqueous Dye-Sensitized Solar Cell Electrolytes Based on a TEMPO/TEMPO+ Redox Couple. *RSC Adv.* **2015**, *5* (34), 26706–26709.
- (121) Fayad, R.; Shoker, T. A.; Ghaddar, T. H. High Photo-Currents with a Zwitterionic Thiocyanate-Free Dye in Aqueous-Based Dye Sensitized Solar Cells. *Dalt. Trans.* **2016**, *45* (13), 5622–5628.
- (122) Daeneke, T.; Uemura, Y.; Duffy, N. W.; Mozer, A. J.; Koumura, N.; Bach, U.; Spiccia, L. Aqueous Dye-Sensitized Solar Cell Electrolytes Based on the Ferricyanide–Ferrocyanide Redox Couple. *Adv. Mater.* **2012**, *24* (9), 1222–1225.
- (123) Ellis, H.; Jiang, R.; Ye, S.; Hagfeldt, A.; Boschloo, G. Development of High Efficiency 100% Aqueous Cobalt Electrolyte Dye-Sensitized Solar Cells. *Phys. Chem. Chem. Phys.* **2016**, *18* (12), 8419–8427.
- (124) Dong, C.; Xiang, W.; Huang, F.; Fu, D.; Huang, W.; Bach, U.; Cheng, Y.-B.; Li, X.; Spiccia, L. Controlling Interfacial Recombination in Aqueous Dye-Sensitized Solar Cells by Octadecyltrichlorosilane Surface Treatment. *Angew. Chemie Int. Ed.* **2014**, *53* (27), 6933–6937.
- (125) Li, L.; Gibson, E. A.; Qin, P.; Boschloo, G.; Gorlov, M.; Hagfeldt, A.; Sun, L. Double-Layered NiO Photocathodes for p-Type DSSCs with Record IPCE. *Adv. Mater.* **2010**, *22* (15), 1759–1762.
- (126) Zhu, H.; Hagfeldt, A.; Boschloo, G. Photoelectrochemistry of Mesoporous NiO Electrodes in Iodide/Triiodide Electrolytes. *J. Phys. Chem. C* **2007**, *111* (47), 17455–17458.
- (127) Perera, I. R.; Daeneke, T.; Makuta, S.; Yu, Z.; Tachibana, Y.; Mishra, A.; Bäuerle, P.; Ohlin, C. A.; Bach, U.; Spiccia, L. Application of the Tris(Acetylacetonato)Iron(III)/(II) Redox Couple in p-Type Dye-Sensitized Solar Cells. *Angew. Chemie Int. Ed.* **2015**, *54* (12), 3758–3762.
- (128) Powar, S.; Daeneke, T.; Ma, M. T.; Fu, D.; Duffy, N. W.; Götz, G.; Weidelener, M.; Mishra, A.; Bäuerle, P.; Spiccia, L.; Bach, U. Highly Efficient P-Type Dye-Sensitized Solar Cells Based on Tris(1,2-Diaminoethane)Cobalt(II)/(III) Electrolytes. *Angew. Chemie Int. Ed.* **2013**, *52* (2), 602–605.
- (129) Xiang, W.; Marlow, J.; Bäuerle, P.; Bach, U.; Spiccia, L. Aqueous P-Type Dye-Sensitized Solar Cells Based on a Tris(1,2-Diaminoethane)Cobalt(II)/(III) Redox Mediator. *Green Chem.* **2016**, *18* (24), 6659–6665.
- (130) Gutmann, V. Solvent Effects on the Reactivities of Organometallic Compounds. *Coord. Chem. Rev.* **1976**, *18* (2), 225–255.
- (131) Fukui, A.; Komiya, R.; Yamanaka, R.; Islam, A.; Han, L. Effect of a Redox Electrolyte in Mixed Solvents on the Photovoltaic Performance of a Dye-Sensitized Solar Cell. *Sol. Energy Mater. Sol. Cells* **2006**, *90* (5), 649–658.
- (132) Hara, K.; Horiguchi, T.; Kinoshita, T.; Sayama, K.; Arakawa, H. Influence of Electrolytes on the Photovoltaic Performance of Organic Dye-Sensitized Nanocrystalline TiO₂ Solar Cells. *Sol. Energy Mater. Sol. Cells* **2001**, *70* (2), 151–161.
- (133) Nazeeruddin, M. K.; Kay, A.; Rodicio, I.; Humphry-Baker, R.; Mueller, E.; Liska, P.; Vlachopoulos, N.; Graetzel, M. Conversion of Light to Electricity by Cis-X₂Bis(2,2'-Bipyridyl-4,4'-Dicarboxylate)-Ruthenium(II) Charge-Transfer Sensitizers (X=C1-, Br-, I-, CN-, and Cis-XSCN-) on Nanocrystalline TiO₂ Electrodes. *J. Am. Chem. Soc.* **1993**, *115* (14), 6382–6390.
- (134) Choi, H.; Han, J.; Kang, M. S.; Song, K.; Ko, J. Aqueous Electrolytes Based Dye-Sensitized Solar Cells Using I⁻/I₃⁻ Redox Couple to Achieve ≥ 4% Power Conversion Efficiency. *Bull. Korean Chem. Soc.* **2014**, *35* (5), 1433–1439.
- (135) Zhang, H.; Qiu, L.; Xu, D.; Zhang, W.; Yan, F. Performance Enhancement for Water Based Dye-Sensitized Solar Cells via Addition of Ionic Surfactants. *J. Mater. Chem. A* **2014**, *2* (7), 2221–2226.
- (136) Bella, F.; Galliano, S.; Falco, M.; Viscardi, G.; Barolo, C.; Grätzel, M.; Gerbaldi, C. Unveiling Iodine-Based Electrolytes Chemistry in Aqueous Dye-Sensitized Solar Cells. *Chem. Sci.* **2016**, *7* (8), 4880–4890.
- (137) Galliano, S.; Bella, F.; Gerbaldi, C.; Falco, M.; Viscardi, G.; Grätzel, M.; Barolo, C. Photoanode/Electrolyte Interface Stability in Aqueous Dye-Sensitized Solar Cells. *Energy Technol.* **2017**, *5* (2), 300–311.
- (138) Kato, N.; Takeda, Y.; Higuchi, K.; Takeichi, A.; Sudo, E.; Tanaka, H.; Motohiro, T.; Sano, T.; Toyoda, T. Degradation Analysis of Dye-Sensitized Solar Cell Module after Long-Term Stability Test under Outdoor Working Condition. *Sol. Energy Mater. Sol. Cells* **2009**, *93* (6–7), 893–897.
- (139) Anthony, J. L.; Brennecke, J. F.; Holbrey, J. D.; Maginn, E. J.; Mantz, R. A.; Rogers, R. D.; Trulove, P. C.; Visser, A. E.; Welton, T. Physicochemical Properties of Ionic Liquids. *Ionic Liquids in Synthesis* **2002**, 41–126.
- (140) Gorlov, M.; Kloo, L. Ionic Liquid Electrolytes for Dye-Sensitized Solar Cells. *Dalt. Trans.* **2008**, *20*, 2655–2666.
- (141) Kubo, W.; Kitamura, T.; Hanabusa, K.; Wada, Y.; Yanagida, S. Quasi-Solid-State Dye-Sensitized Solar Cells Using Room Temperature Molten Salts and a Low Molecular Weight Gelator. *Chem. Commun.* **2002**, *4*, 374–375.
- (142) Kambe, S.; Nakade, S.; Kitamura, T.; Wada, Y.; Yanagida, S. Influence of the Electrolytes on Electron Transport in Mesoporous TiO₂–Electrolyte Systems. *J. Phys. Chem. B* **2002**, *106* (11), 2967–2972.
- (143) Wang, P.; Wenger, B.; Humphry-Baker, R.; Moser, J.-E.; Tscherscher, J.; Kantelechner, W.; Mezger, J.; Stoyanov, E. V.; Zakeeruddin, S. M.; Grätzel, M. Charge Separation and Efficient Light Energy Conversion in Sensitized Mesoscopic Solar Cells Based on Binary Ionic Liquids. *J. Am. Chem. Soc.* **2005**, *127* (18), 6850–6856.
- (144) Hao, F.; Lin, H.; Liu, Y.; Li, J. Anionic Structure-Dependent Photoelectrochemical Responses of Dye-Sensitized Solar Cells Based on a Binary Ionic Liquid Electrolyte. *Phys. Chem. Chem. Phys.* **2011**, *13* (14), 6416–6422.
- (145) Kuang, D.; Klein, C.; Zhang, Z.; Ito, S.; Moser, J.-E.; Zakeeruddin, S. M.; Grätzel, M. Stable, High-Efficiency Ionic-Liquid-Based Mesoscopic Dye-Sensitized Solar Cells. *Small* **2007**, *3* (12), 2094–2102.
- (146) Yoshida, Y.; Muroi, K.; Otsuka, A.; Saito, G.; Takahashi, M.; Yoko, T. 1-Ethyl-3-Methylimidazolium Based Ionic Liquids Containing Cyano Groups: Synthesis, Characterization, and Crystal Structure. *Inorg. Chem.* **2004**, *43* (4), 1458–1462.
- (147) Fabregat-Santiago, F.; Bisquert, J.; Palomares, E.; Otero, L.; Kuang, D.; Zakeeruddin, S. M.; Grätzel, M. Correlation between Photovoltaic Performance and Impedance Spectroscopy of Dye-Sensitized Solar Cells Based on Ionic Liquids. *J. Phys. Chem. C* **2007**, *111* (17), 6550–6560.
- (148) Matsumoto, H.; Matsuda, T.; Tsuda, T.; Hagiwara, R.; Ito, Y.; Miyazaki, Y. The Application of Room Temperature Molten Salt with Low Viscosity to the Electrolyte for Dye-Sensitized Solar Cell. *Chem. Lett.* **2001**, *30* (1), 26–27.
- (149) Sun, H.; Hoffman, M. Z. Reductive Quenching of the Excited States of Ruthenium(II) Complexes Containing 2,2'-Bipyridine, 2,2'-Bipyrazine, and 2,2'-Bipyrimidine Ligands. *J. Phys. Chem.* **1994**, *98* (45), 11719–11726.
- (150) Shi, D.; Pootrakulchote, N.; Li, R.; Guo, J.; Wang, Y.; Zakeeruddin, S. M.; Grätzel, M.; Wang, P. New Efficiency Records for Stable Dye-Sensitized Solar Cells with Low-Volatility and Ionic Liquid Electrolytes. *J. Phys. Chem. C* **2008**, *112* (44), 17046–17050.
- (151) Bousrez, G.; Renier, O.; Adranno, B.; Smetana, V.; Mudring, A.-V. Ionic Liquid-Based Dye-Sensitized Solar Cells—Insights into Electrolyte and Redox Mediator Design. *ACS Sustain. Chem. Eng.* **2021**, *9* (24), 8107–8114.
- (152) Boschloo, G.; Häggman, L.; Hagfeldt, A. Quantification of the Effect of 4-Tert-Butylpyridine Addition to I⁻/I₃⁻ Redox Electrolytes in

- Dye-Sensitized Nanostructured TiO₂ Solar Cells. *J. Phys. Chem. B* **2006**, *110* (26), 13144–13150.
- (153) Nakade, S.; Kanzaki, T.; Kubo, W.; Kitamura, T.; Wada, Y.; Yanagida, S. Role of Electrolytes on Charge Recombination in Dye-Sensitized TiO₂ Solar Cell (1): The Case of Solar Cells Using the I⁻/I₃⁻ Redox Couple. *J. Phys. Chem. B* **2005**, *109* (8), 3480–3487.
- (154) Schlichthörl, G.; Huang, S. Y.; Sprague, J.; Frank, A. J. Band Edge Movement and Recombination Kinetics in Dye-Sensitized Nanocrystalline TiO₂ Solar Cells: A Study by Intensity Modulated Photovoltage Spectroscopy. *J. Phys. Chem. B* **1997**, *101* (41), 8141–8155.
- (155) Huang, S. Y.; Schlichthörl, G.; Nozik, A. J.; Grätzel, M.; Frank, A. J. Charge Recombination in Dye-Sensitized Nanocrystalline TiO₂ Solar Cells. *J. Phys. Chem. B* **1997**, *101* (14), 2576–2582.
- (156) Johnson, A. L.; Muetterties, E. L.; Stohr, J.; Sette, F. Chemisorption Geometry of Pyridine on Platinum(111) by NEXAFS. *J. Phys. Chem.* **1985**, *89* (19), 4071–4075.
- (157) Krauskopf, E. K.; Rice-Jackson, L. M.; Wiecekowsky, A. Pyridine Adsorption on Polycrystalline Platinum Studied by the Radioactive-Labeling Method. *Langmuir* **1990**, *6* (5), 970–973.
- (158) Kim, J.-Y.; Kim, J. Y.; Lee, D.-K.; Kim, B.; Kim, H.; Ko, M. J. Importance of 4-Tert-Butylpyridine in Electrolyte for Dye-Sensitized Solar Cells Employing SnO₂ Electrode. *J. Phys. Chem. C* **2012**, *116* (43), 22759–22766.
- (159) Hoffeditz, W. L.; Katz, M. J.; Deria, P.; Cutsail, G. E., III; Pellin, M. J.; Farha, O. K.; Hupp, J. T. One Electron Changes Everything. A Multispecies Copper Redox Shuttle for Dye-Sensitized Solar Cells. *J. Phys. Chem. C* **2016**, *120* (7), 3731–3740.
- (160) Ferdowsi, P.; Saygili, Y.; Zakeeruddin, S. M.; Mokhtari, J.; Grätzel, M.; Hagfeldt, A.; Kavan, L. Alternative Bases to 4-Tert-Butylpyridine for Dye-Sensitized Solar Cells Employing Copper Redox Mediator. *Electrochim. Acta* **2018**, *265*, 194–201.
- (161) Buncel, E.; Joly, H. A.; Jones, J. R. Proton Transfer from Imidazole, Benzimidazole, and Their 1-Alkyl Derivatives. FMO Analysis of the Effect of Methyl and Benzo Substitution. *Can. J. Chem.* **1986**, *64* (6), 1240–1245.
- (162) Yu, Z.; Gorlov, M.; Boschloo, G.; Kloo, L. Synergistic Effect of N-Methylbenzimidazole and Guanidinium Thiocyanate on the Performance of Dye-Sensitized Solar Cells Based on Ionic Liquid Electrolytes. *J. Phys. Chem. C* **2010**, *114* (50), 22330–22337.
- (163) Zhang, C.; Dai, J.; Huo, Z.; Pan, X.; Hu, L.; Kong, F.; Huang, Y.; Sui, Y.; Fang, X.; Wang, K.; Dai, S. Influence of 1-Methylbenzimidazole Interactions with Li⁺ and TiO₂ on the Performance of Dye-Sensitized Solar Cells. *Electrochim. Acta* **2008**, *53* (17), 5503–5508.
- (164) Furer, S. O.; Milhaisen, R. A.; Kashif, M. K.; Raga, S. R.; Acharya, S. S.; Forsyth, C.; Liu, M.; Frazer, L.; Duffy, N. W.; Ohlin, C. A.; Funston, A. M.; Tachibana, Y.; Bach, U. The Performance-Determining Role of Lewis Bases in Dye-Sensitized Solar Cells Employing Copper-Bisphenanthroline Redox Mediators. *Adv. Energy Mater.* **2020**, *10* (37), 2002067.
- (165) Kannankutty, K.; Chen, C.-C.; Nguyen, V. S.; Lin, Y.-C.; Chou, H.-H.; Yeh, C.-Y.; Wei, T.-C. Tert-Butylpyridine Coordination with [Cu(Dmp)₂]^{2+/+} Redox Couple and Its Connection to the Stability of the Dye-Sensitized Solar Cell. *ACS Appl. Mater. Interfaces* **2020**, *12* (5), 5812–5819.
- (166) Saygili, Y.; Stojanovic, M.; Michaels, H.; Tjepelt, J.; Teuscher, J.; Massaro, A.; Pavone, M.; Giordano, F.; Zakeeruddin, S. M.; Boschloo, G.; Moser, J.-E.; Grätzel, M.; Muñoz-García, A. B.; Hagfeldt, A.; Freitag, M. Effect of Coordination Sphere Geometry of Copper Redox Mediators on Regeneration and Recombination Behavior in Dye-Sensitized Solar Cell Applications. *ACS Appl. Energy Mater.* **2018**, *1* (9), 4950–4962.
- (167) Zhang, C.; Huang, Y.; Huo, Z.; Chen, S.; Dai, S. Photoelectrochemical Effects of Guanidinium Thiocyanate on Dye-Sensitized Solar Cell Performance and Stability. *J. Phys. Chem. C* **2009**, *113* (52), 21779–21783.
- (168) Kopidakis, N.; Neale, N. R.; Frank, A. J. Effect of an Adsorbent on Recombination and Band-Edge Movement in Dye-Sensitized TiO₂ Solar Cells: Evidence for Surface Passivation. *J. Phys. Chem. B* **2006**, *110* (25), 12485–12489.
- (169) Kopidakis, N.; Benkstein, K. D.; van de Lagemaat, J.; Frank, A. J. Transport-Limited Recombination of Photocarriers in Dye-Sensitized Nanocrystalline TiO₂ Solar Cells. *J. Phys. Chem. B* **2003**, *107* (41), 11307–11315.
- (170) Kim, C. K.; Choi, I. T.; Kang, S. H.; Kim, H. K. Anchovy-Derived Nitrogen and Sulfur Co-Doped Porous Carbon Materials for High-Performance Supercapacitors and Dye-Sensitized Solar Cells. *RSC Adv.* **2017**, *7* (57), 35565–35574.
- (171) Zhang, L.; Yang, X.; Wang, W.; Gurzadyan, G. G.; Li, J.; Li, X.; An, J.; Yu, Z.; Wang, H.; Cai, B.; Hagfeldt, A.; Sun, L. 13.6% Efficient Organic Dye-Sensitized Solar Cells by Minimizing Energy Losses of the Excited State. *ACS Energy Lett.* **2019**, *4* (4), 943–951.
- (172) Ren, Y.; Flores-Díaz, N.; Zhang, D.; Cao, Y.; Decoppet, J. D.; Fish, G. C.; Moser, J. E.; Zakeeruddin, S. M.; Wang, P.; Hagfeldt, A.; Grätzel, M. Blue Photosensitizer with Copper(II/I) Redox Mediator for Efficient and Stable Dye-Sensitized Solar Cells. *Adv. Funct. Mater.* **2020**, *30* (50), 2004804.
- (173) Michaels, H.; Benesperi, I.; Freitag, M. Challenges and Prospects of Ambient Hybrid Solar Cell Applications. *Chem. Sci.* **2021**, *12* (14), 5002–5015.
- (174) Tingare, Y. S.; Vinh, N. S.; Chou, H.-H.; Liu, Y.-C.; Long, Y.-S.; Wu, T.-C.; Wei, T.-C.; Yeh, C.-Y. New Acetylene-Bridged 9,10-Conjugated Anthracene Sensitizers: Application in Outdoor and Indoor Dye-Sensitized Solar Cells. *Adv. Energy Mater.* **2017**, *7* (18), 1700032.
- (175) Hora, C.; Santos, F.; Sales, M. G. F.; Ivanou, D.; Mendes, A. Dye-Sensitized Solar Cells for Efficient Solar and Artificial Light Conversion. *ACS Sustain. Chem. Eng.* **2019**, *7* (15), 13464–13470.
- (176) Venkatesan, S.; Lin, W.-H.; Teng, H.; Lee, Y.-L. High-Efficiency Bifacial Dye-Sensitized Solar Cells for Application under Indoor Light Conditions. *ACS Appl. Mater. Interfaces* **2019**, *11* (45), 42780–42789.
- (177) Freitag, M.; Teuscher, J.; Saygili, Y.; Zhang, X.; Giordano, F.; Liska, P.; Hua, J.; Zakeeruddin, S. M.; Moser, J.-E.; Grätzel, M.; Hagfeldt, A. Dye-Sensitized Solar Cells for Efficient Power Generation under Ambient Lighting. *Nat. Photonics* **2017**, *11* (6), 372–378.
- (178) Tang, Y.; Wang, Y.; Li, X.; Ågren, H.; Zhu, W.-H.; Xie, Y. Porphyrins Containing a Triphenylamine Donor and up to Eight Alkoxy Chains for Dye-Sensitized Solar Cells: A High Efficiency of 10.9%. *ACS Appl. Mater. Interfaces* **2015**, *7* (50), 27976–27985.
- (179) Bisht, R.; Mele Kavungathodi, M. F.; Nithyanandhan, J. Indenoquinoline-Based Unsymmetrical Squaraine Dyes for Near-Infrared Absorption: Investigating the Steric and Electronic Effects in Dye-Sensitized Solar Cells. *Chem. - A Eur. J.* **2018**, *24* (61), 16368–16378.
- (180) Wang, P.; Yang, L.; Wu, H.; Cao, Y.; Zhang, J.; Xu, N.; Chen, S.; Decoppet, J. D.; Zakeeruddin, S. M.; Grätzel, M. Stable and Efficient Organic Dye-Sensitized Solar Cell Based on Ionic Liquid Electrolyte. *Joule* **2018**, *2* (10), 2145–2153.
- (181) Kim, C. K.; Kim, H. M.; Aftabuzzaman, M.; Jeon, I.-Y.; Kang, S. H.; Eom, Y. K.; Baek, J. B.; Kim, H. K. Comparative Study of Edge-Functionalized Graphene Nanoplatelets as Metal-Free Counter Electrodes for Highly Efficient Dye-Sensitized Solar Cells. *Mater. Today Energy* **2018**, *9*, 67–73.
- (182) Ji, J.-M.; Kim, C. K.; Kim, H. K. Well-Dispersed Te-Doped Mesoporous Carbons as Pt-Free Counter Electrodes for High-Performance Dye-Sensitized Solar Cells. *Dalt. Trans.* **2021**, *50* (27), 9399–9409.